

Identifying Therapeutic Targets for Triple-Negative Breast Cancer using a Novel Mathematical Model of the Tumor Microenvironment

Authors: Kyle Adams¹, Julia Bruner², Salma Ameziane¹, Ashley Brown³, Mohammed Gbadamosi⁴, Helen Moore⁵.

1. Department of Mathematics, College of Liberal Arts and Sciences, University of Florida, Gainesville, Florida, USA.
2. Department of Surgery, College of Medicine, University of Florida, Gainesville, Florida, USA.
3. Department of Molecular Genetics and Microbiology, College of Medicine, University of Florida, Gainesville, Florida, USA.
4. Department of Pharmacotherapy and Translational Research, College of Pharmacy, University of Florida, Gainesville, Florida, USA.
5. Department of Medicine, College of Medicine, University of Florida, Gainesville, Florida, USA.

Abstract

Triple-negative breast cancer (TNBC) is an aggressive disease with high mortality and limited treatment options, due to its lack of receptors that have targeted therapies available. The tumor microenvironment (TME) plays a critical role in TNBC progression and therapeutic resistance. In this work, we developed a novel mathematical model to describe key cellular interactions within the TNBC TME, informed by current literature and expert input. Our model consists of a system of ordinary differential equations representing five interacting cell populations: M2 macrophages, cancer-associated fibroblasts, TNBC tumor cells, cytotoxic T lymphocytes, and regulatory T cells. We performed global sensitivity analysis to determine which model parameters most strongly influence tumor burden over a clinically-relevant treatment timeframe. The pathways associated with the most-influential parameters correspond to biological mechanisms that are consistent with known and emerging therapeutic strategies in TNBC, including stromal-mediated tumor support. These results highlight key regulatory interactions within the TNBC TME and provide a quantitative framework for hypothesis generation and future investigation of combination treatment strategies.

Introduction

In 157 countries out of the 185 studied by the Global Cancer Observatory, breast cancer was the most-commonly diagnosed cancer in women in 2022.¹ The American Cancer Society estimates that a woman in the United States has approximately a 1 in 8 chance of developing breast cancer in her lifetime.² This disease affects women of all races and ethnicities.³ The importance of breast cancer research is impossible to overstate.

In this work, we focus on triple-negative breast cancer (TNBC) due to its aggressiveness, its low survival rates, and the fact that it is the most immunogenic of the breast cancer subtypes.⁴ Approximately 10-15% of all breast cancers are triple-negative, which refers to cancer cells that lack three key receptors: estrogen receptor (ER), progesterone receptor (PR), and HER2 receptor.² Depending on the cancer stage at diagnosis, chemotherapy, immunotherapy, radiation, and surgery are current treatment options for people with TNBC.² However, due to negativity for ER, PR, and HER2, TNBC tumors will not respond

to therapies that are available to target these receptors, and so there are fewer treatment options compared to other breast cancer subtypes.²

The TNBC tumor microenvironment (TME) has been an area of recent focus.^{4,5} Our goal in this work was to contribute to this research by developing a mechanistic math model describing specific components of the TME of TNBC. Different types of mathematical models have been widely used in medicine with goals such as predicting the hospitalization needs of COVID-19 patients,⁶ optimizing treatment schedules for cancer patients,^{7,8} and exploring treatment resistance.⁹ We briefly review prior mathematical models for breast cancer and discuss the novel features of our model. Our model consists of a system of ordinary differential equations (ODEs) that describe the dynamics among M2 macrophages (M2), cancer-associated fibroblasts (CAFs), triple-negative breast cancer tumor cells (B), activated cytotoxic T lymphocytes (CTL, T_C), regulatory T cells (Tregs, T_R). Recently, immunotherapy has shown significant potential as a treatment for TNBC,¹⁰ which underscores the importance of focusing on the TME.

In this work, we share the foundations and justifications for our model, and describe the specific cell populations included and their interactions in the TNBC TME. We also perform global sensitivity analysis and discuss the implications of the most-influential parameters identified.

While this model does not explicitly simulate therapeutic interventions, its goal is to identify biologically-influential pathways that regulate tumor burden over clinically-relevant timescales. Parameters identified as highly influential through sensitivity analysis should be interpreted as indicators of mechanistic importance rather than definite therapeutic efficacy. Consequently, the results of this study are intended to generate hypotheses regarding promising intervention strategies, which may be evaluated in future computational, experimental, or clinical studies.

Mechanistic Mathematical Models Of Breast Cancer

Many mechanistic math models for breast cancer have been proposed, with different approaches and goals. These include fractional models, ODE models, partial differential equation (PDE) models, mixed ODE/PDE models, and agent-based models (ABMs). Akman et al. developed an ODE model to investigate the relationship between diet and anti-hormonal therapy.¹¹ Schmiester et al. developed and calibrated a coupled-ODE model in an effort to personalize luminal-B breast cancer treatment.¹² An ODE model by Abernathy et al. describes global dynamics of breast cancer through an immune-cancer competition model, which was later used to understand optimal immune response rates.^{13,14} This model was later the foundation for a fractional model built by Solís-Pérez et al.¹⁵ Chavada et al. developed and analyzed a fractional model to describe breast cancer stages.¹⁶ Aldwoah et al. modeled breast cancer progression using a fractional and stochastic model.¹⁷ An ODE model by Jarrett et al. focuses on HER2+ breast cancer and includes effects from trastuzumab,¹⁸ a common targeted therapy for HER2+ breast cancer. An ODE model that explores drug regimens of doxorubicin and cyclophosphamide, methotrexate, and fluorouracil therapy was proposed by Roe-Dale et al.¹⁹ Wei published an ODE model for TNBC that includes natural killer cells, CTLs, circulating lymphocytes, PD-L1 and PD-1 concentration, PD-L1 on tumor cells, and an anti-PD-L1 drug to explore immune checkpoint inhibitors.²⁰ Wei also published a mathematical model of ER-positive breast cancer with two treatments: AZD9496 and palbociclib,²¹ that was further analyzed by Nave.²² Mehdizadeh et al proposed an ODE model that includes proliferative cancer cells, quiescent cancer cells, CD8+ T cells, and natural killer cells to investigate immunological dormancy of TNBC.²³ Mirzaei et al. developed an ODE model of tumor-immune dynamics to study the effect of immune cell infiltration, particularly macrophages, CTLs, helper T cells, Tregs, adipocytes, necrotic cells, and various cytokines.²⁴ The authors later analyzed dynamics of their model using murine data.²⁵ Arulraj et al. developed a quantitative systems pharmacology model of TNBC to study how antigen presentation and cytotoxic T-cell activation influence response to PD-1 therapy.²⁶ Maiti et al. developed an ODE mechanistic model to investigate extracellular matrix deprivation in breast cancer metastasis.²⁷ Akil et al. applied optimal control to their ODE model of ER+ breast cancer, using ketogenic diet, hormonal therapy, and immunotherapy as their controls.²⁸ Enderling et al. proposed a PDE model

describing breast cancer tumor growth and invasion to investigate radiotherapy and local recurrence.²⁹ Knútsdóttir et al. proposed a PDE model to aid in drug design by modeling macrophages and a few of their cytokine secretions.³⁰ Christenson et al. developed a PDE model to personalize neoadjuvant chemotherapy regimens using digital twins,³¹ and then studied rapid calibration using proper orthogonal decomposition.³² Weis et al used a reaction-diffusion PDE model to predict the response of breast-cancer patients to neoadjuvant therapy.³³ Miniere et al. proposed a reaction-diffusion PDE model to predict the response of cancer cells to doxorubicin treatment.³⁴ Norton et al. developed an ABM to understand the relationship between expression of the biomarker CCR5, cancer stem cells, and hypoxia in TNBC.³⁵ Each of these models differs from ours in the cell populations included. Some of these models include a treatment, whereas the goal of our work was to establish a model of key TNBC TME dynamics for analysis of key drivers of tumor size, and to expand the model and further analyze it later.

Model and Justifications

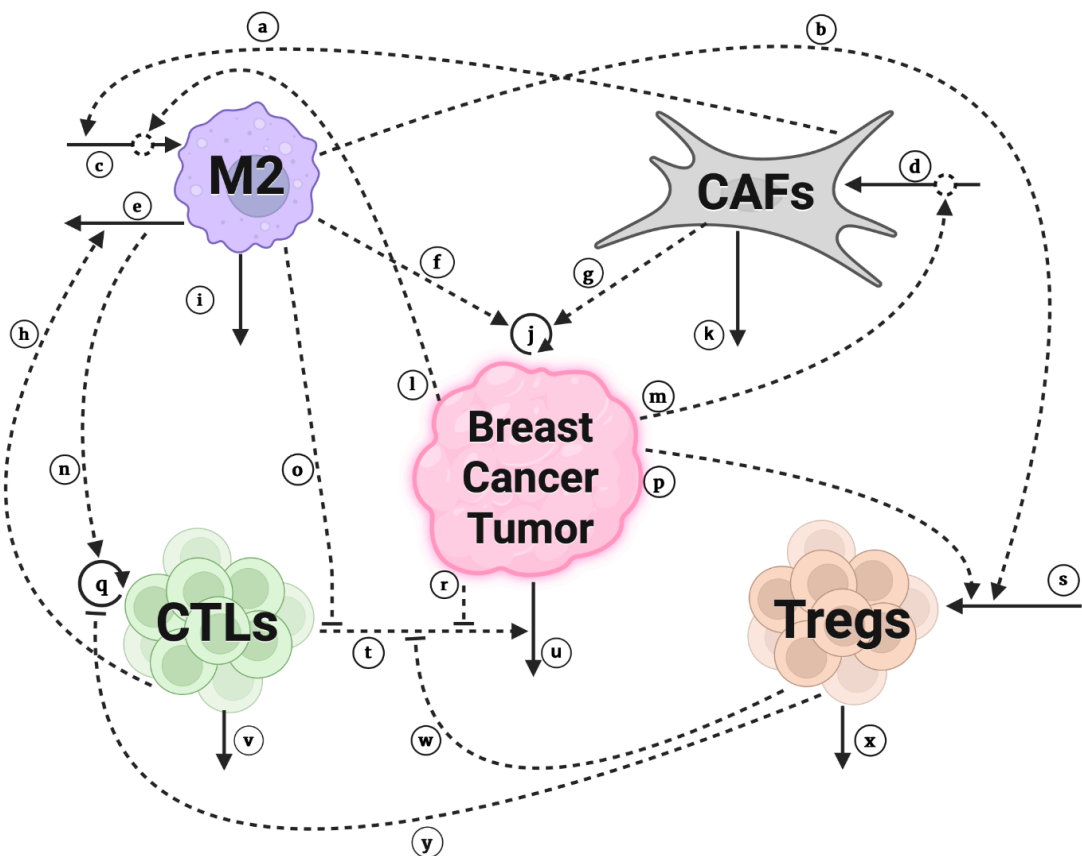


Figure 1. Each of the five cell populations, M2 macrophages (M2), cancer-associated fibroblasts (CAFs), triple-negative breast cancer tumor cells (breast cancer tumor), activated cytotoxic T lymphocytes (CTLs), and regulatory T cells (Tregs), is represented by a shape and its abbreviation. Solid arrows represent a change in cell number. Solid arrows pointing away from a cell depict loss of that cell's population (due to natural death, or repolarization in the case of arrow e). Solid arrows pointing toward a cell population represent an increase in that population's number. This could be due to polarization, differentiation (specifically normal fibroblasts differentiating to CAFs in arrow d), recruitment, or proliferation in the case of a circular solid arrow. Dotted curves with arrows represent a boosting effect on

the mechanism they are pointing to. Dotted curves with a flat end represent an inhibition effect on the mechanism they are pointing to. Each mechanism is labeled and discussed in detail in section **blank**. This figure was created with BioRender.com.

Cell Populations & Dynamics

The tumor microenvironment of triple-negative breast cancer is complex, with many types of cells contributing pro-tumor or anti-tumor effects. In this work, our goal is to establish a simple model capturing the dynamics of the most important cell populations in the TNBC TME. Our model is small by design, and is representative of “net effects” that include effects from cells and mechanisms that are not explicitly represented in the model. We included cell populations if they were clearly key players in TNBC, if their importance had scientific consensus, and if their dynamics may be affected by current or hypothesized treatments.

M2 Macrophages (M2)

Several studies have indicated the important roles that tumor-associated macrophages (TAMs) play in the TME of TNBC.³⁶⁻³⁹ TAMs originate from bone marrow-derived monocytes which circulate in peripheral blood before being recruited to the TME by tumor cells or by host immune cells. In tissue, they differentiate into macrophages of different phenotypic classes, in a process called polarization. TAMs may refer to both M1-like macrophages, which have anti-tumor, pro-inflammatory activity, and M2-like macrophages, which have pro-tumor, anti-inflammatory activity. While there is a spectrum of macrophage phenotypes,⁴⁰ in our model, we labeled all pro-tumor macrophages as M2 macrophages. That is, M2 macrophages in our model could refer to either an M2 macrophage or an M2-like macrophage. We included M2 macrophages in our model as they make up a majority of TAM populations within tumors,⁴¹ and the proportion of TAMs that are M2 macrophages has been reported to increase as the tumor progresses.⁴² The source of M2 macrophages (**arrow c**) represents both direct polarization of undifferentiated monocytes into M2 macrophages as well as the repolarization of M1 macrophages to the M2 phenotype. In either case, the source of tumor-associated M2 macrophages (**arrow c**) is dependent on the presence of tumor cells (**arrow l**). Polarization of TAMs toward the M2 phenotype occurs in the presence of anti-inflammatory cytokines and signals from other cell types including CAFs (**arrow a**) and TNBC tumor cells (**arrow l**). Cohen et al.⁴³ showed that the protein Chi3L1 secreted by CAFs causes macrophages to migrate to the TME and polarizes them to be M2. Several studies also discuss the release of TGF- β from CAFs,^{44,45} which has been shown to polarize M1 to M2 macrophages.^{4,46,47} Breast cancer cells secrete IL-2, IL-10, TGF- β , and M-CSF, which polarize M1-like macrophages to M2 macrophages.^{4,37} Also, TNBC specifically secretes more G-CSF compared to other breast cancer subtypes, which is also a promoter of M1 to M2 polarization.⁴⁸

In the TME, M2 macrophages suppress CTL activity (**arrow o**) through several mechanisms. Multiple immune checkpoint ligands, including PDL1 and B7-H4, have been implicated in blocking CTL activity.⁴⁹⁻⁵¹ M2 macrophages also produce TGF- β , which inhibits CTL function.⁵² M2 macrophages can also influence CTL activity by depleting L-arginine, as discussed previously. M2 macrophages can inhibit CTL proliferation,⁵³ but to simplify the model and to reduce potential structural identifiability issues, we include this effect in our estimate for parameters involved in **pathway o**. There are at least three mechanisms through which M2 macrophages may inhibit CTL proliferation. First, a murine study found that PGRN derived from a breast tumor polarized TAMs to M2 macrophages, which then inhibited proliferation of CTLs mediated by ICAM-1.⁵⁴ Second, L-arginine has been shown to be necessary for CTL proliferation,⁵⁵ but M2 macrophages metabolize L-arginine by expressing Arg-1, out-competing T cells of this necessary resource to proliferate.⁵⁶ The latter pathway is currently being researched as a possible target for TNBC therapy.⁵⁷ Last, M2 macrophages can release TGF- β ,⁴² which can inhibit CTL proliferation.⁵⁸

M2 macrophages also recruit Tregs to the TME (**arrow b**). M2 macrophages secrete anti-inflammatory cytokines and chemokines, including TGF- β , which induce differentiation of naive

helper T cells into Tregs.⁵⁹ In ovarian cancer studies, macrophage-derived chemokine CCL22 results in the recruitment of peripheral Tregs.⁶⁰ Further, TAMs, which tend to be M2 macrophages, especially as the tumor progresses,⁴² secrete growth factors including BFGF-2, EGF, PDGF, and TGF- β , which are responsible for tumor cell proliferation (**arrow f**).⁴ The natural loss of M2 macrophages upon completion of a finite lifespan is represented by **arrow i**.

We chose to capture the dynamics of M1 macrophages indirectly by including the possible repolarization of M2 macrophages to M1 macrophages (**arrow e**). Repolarization of M2 macrophages to M1 macrophages has been shown to occur in osteosarcoma,⁶¹ and with a treatment (matairesinol) in triple-negative breast cancer.^{61,62} Yuan et al. found that higher infiltration of TAMs in TNBC is associated with a “significantly higher risk of distant metastasis”, and lower rates of overall survival (OS) and disease-free survival (DFS).³⁹ Modelling the TNBC TME with both M1 and M2 macrophages is useful as conversion of TAMs to M1-like macrophages is a potential new therapy in triple negative breast cancer.⁶³

Cancer-Associated Fibroblasts (CAFs)

CAFs are resident fibroblasts that are activated by tumor cells toward a pro-tumor state (**arrow d**).^{64,65} The transformation from normal fibroblasts to CAFs occurs in response to tumor-secreted factors including TGF- β , PDGF, and CXCL12 (**arrow m, d**).^{66,67} In the TME, CAFs’ secretion of TGF- β and CXCL12 increases proliferation of breast cancer cells leading to enhanced tumor growth (**arrow g**).⁶⁷ As mentioned, CAFs also increase the source of M2 macrophages (**arrow a**). CAFs’ secretion of Chi3L1 causes macrophages and monocytes to migrate to the TME and polarize toward the M2 phenotype.⁴³ TGF- β secretion has also been shown to play a role in the repolarization of M1 macrophages to the M2 state.⁴⁴⁻⁴⁷ The natural loss of CAFs upon completion of a finite lifespan is represented by **arrow k**.

Because of these effects, there has been growing interest in the role CAFs play in the tumor microenvironment of TNBC.⁶⁸⁻⁷⁰ CAFs are found in several cancers,⁶⁴ and in TNBC there is a correlation between CAFs and tumor aggressiveness and disease recurrence.⁷¹ CAFs are also implicated in macrophage dynamics, immune suppression, and immune escape.⁶⁸ In some cases CAFs have been shown to induce resistance to treatments including radiotherapy, hormonal therapy, and chemotherapy.⁷⁰ Since TNBC often exhibits chemotherapeutic resistance and has an immunosuppressive tumor microenvironment, CAFs have been investigated recently as a therapeutic target to address these challenges.⁷²

Cytotoxic T lymphocytes (CTLs)

Cytotoxic T lymphocytes, also known as CD8+ T cells, are a subset of tumor-infiltrating lymphocytes (TILs) responsible for direct immune-mediated killing of damaged, infected, or cancerous host cells. CTLs are critical players in the TME; they are a valuable prognostic metric and vital to anti-PD-1 therapy.^{73,74} In this model, we specifically chose to model activated CD8+ T cells, that is, CD8+ T cells that exhibit functional cytotoxic activity against tumor cells. Upon recognition of tumor antigens, and with costimulatory signals from other immune cells, CTLs become activated, proliferate (**arrow q**), and target cancer cells for death. CTLs kill tumor cells (**arrow t**) using the perforin-granzyme pathway and through expression of death ligands, including Fas ligand (FasL) and TNF-related apoptosis inducing ligand (TRAIL).⁷⁵ However, CTL cytotoxic activity is suppressed by several cells in the immunosuppressive TME, including M2 macrophages (**arrow o**), Tregs (**arrow w**), and breast cancer tumor cells themselves (**arrow r**). Breast cancer cells can upregulate PD-L1 expression, resulting in binding to PD-1 receptors on CTLs, inactivating the CTLs. It is estimated that 30% to 50% of all breast cancers have upregulated PD-L1.⁷⁶ The suppressive roles of M2 macrophages and Tregs are discussed in their respective descriptions in the model dynamics section.

Although M1 macrophages and CD4+ T cells are not explicitly included as cell populations in our model, their downstream effects in CTL activation are captured by **arrow n**. M1 macrophages are classically-activated antigen-presenting cells; once M2 macrophages are polarized to M1 macrophages (**arrow e**), they participate in T cell activation and clonal expansion (**arrow n**).⁷⁷ Another TME dynamic implicitly captured is CTLs boosting polarization of M2 macrophages to M1 macrophages (**arrow h**).

Because the TME is generally immunosuppressive, the rate of polarization of M2 to M1 macrophages in vivo is low. However, administration of immunotherapies leading to T cell activation and engagement with tumor cells leads to greater tumor infiltration with M1 macrophages.^{78,79} While we represent this effect with **arrow h**, we note that this observed increase in macrophages is also likely to occur through recruitment of M1 macrophages. **Arrow v** represents the loss of CTLs, as they have a finite lifespan.⁸⁰

Regulatory T Cells (Tregs)

Tregs, or CD4+CD25+FOXP3+ T cells, play an integral role in tumor progression.^{81,82,83} Labeling studies by Vukmanovic-Sejic et al. in healthy volunteers supported the hypothesis that Tregs are limited in their self-renewal, and are likely continuously recruited from a pool of CD4+ memory T cells.⁸⁴ Thus we assume that the Tregs in our model are recruited to the TME from a source outside of our model. Tregs are generally recruited to the TME via chemokines (**arrow s**).⁸⁵ In claudin-low breast cancers, which are low in tight junction and adhesion proteins, and are generally found in patients with TNBC, Tregs are recruited through the chemokine CXCL12 generated by the tumor (**arrow p**).⁸⁶ Chang et al. found that colon cancer cells express CCL5 which recruits Tregs through CCR5,⁸⁷ a mechanism further evaluated in breast cancer.⁸⁸ Tregs are also recruited by cytokines that M2 macrophages release.⁵⁹

There is an association between increased Treg infiltration of a TNBC tumor and decreased CTL infiltration of the tumor.⁸⁹ Sawant et al. showed that subsets of Treg populations can express IL-10 and IL-35, leading to exhaustion of CD8+ tumor-infiltrating lymphocytes (**arrow w**).⁹⁰ Competition for IL-2 between Tregs and CTLs has been shown to directly inhibit CTL proliferation (**arrow y**).⁹¹ Tay et al. reviewed Tregs as immunotherapy targets in cancer, supported by Tregs' potential to outcompete conventional T-cells for IL-2.⁹² **Arrow x** represents the loss of Tregs, as they have a finite lifespan.⁸⁰

The Model

$$\begin{aligned}
 (1) \frac{dM_2}{dt} &= \underbrace{\left(\frac{\alpha_{B2}B}{\beta_{B2} + B}\right)}_{c,1} \underbrace{\left(1 + \frac{\alpha_{F2}F}{\beta_{F2} + F}\right)}_{a} - \underbrace{\gamma_2 M_2}_{e} \underbrace{\left(1 + \frac{\alpha_{C2}T_C}{\beta_{C2} + T_C}\right)}_{h} - \underbrace{\delta_2 M_2}_{i} \\
 (2) \frac{dF}{dt} &= \underbrace{\sigma_F B \left(1 - \frac{F}{K_F}\right)}_{d,m} - \underbrace{\delta_F F}_{k} \\
 (3) \frac{dB}{dt} &= p_B B \left(1 - \frac{B}{K_B}\right) \underbrace{\left(1 + \frac{\alpha_{2B}M_2}{\beta_{2B} + M_2}\right)}_{j} \underbrace{\left(1 + \frac{\alpha_{FB}F}{\beta_{FB} + F}\right)}_{f} - \underbrace{\delta_B B}_{u} \underbrace{\left(1 + \frac{\alpha_{CB}T_C}{\beta_{CB} + T_C}\right)}_{t} \underbrace{\left[\left(1 - \frac{\alpha_{2CB}M_2}{\beta_{2CB} + M_2}\right) \left(1 - \frac{\alpha_{BCB}B}{\beta_{BCB} + B}\right) \left(1 - \frac{\alpha_{RCB}T_R}{\beta_{RCB} + T_R}\right) \right]}_{o} \underbrace{\left(1 - \frac{\alpha_{RCB}T_R}{\beta_{RCB} + T_R}\right)}_{r} \underbrace{\left(1 - \frac{\alpha_{RCB}T_R}{\beta_{RCB} + T_R}\right)}_{w} \\
 (4) \frac{dT_C}{dt} &= p_C T_C \left(1 - \frac{T_C}{K_C}\right) \underbrace{\left(1 + \frac{\alpha_{2C}M_2}{\beta_{2C} + M_2}\right)}_{q} \underbrace{\left(1 - \frac{\alpha_{RC}T_R}{\beta_{RC} + T_R}\right)}_{n} \underbrace{\left(1 - \frac{\alpha_{RC}T_R}{\beta_{RC} + T_R}\right)}_{y} - \underbrace{\delta_C T_C}_{v} \\
 (5) \frac{dT_R}{dt} &= \underbrace{\sigma_R}_{s} \underbrace{\left(1 + \frac{\alpha_{2R}M_2}{\beta_{2R} + M_2}\right)}_{b} \underbrace{\left(1 + \frac{\alpha_{BR}B}{\beta_{BR} + B}\right)}_{p} - \underbrace{\delta_R T_R}_{x}
 \end{aligned}$$

Model Assumptions

Our model of the TNBC TME consists of a system of five ODEs, one for each cell population. A large majority of TNBC patients are diagnosed at Stages I, II, or III of the disease; the most common stage at diagnosis is Stage II.⁹³ We have chosen to model TNBC beginning at Stage II, which is reflected in certain choices of the model diagram and equations discussed below. Because we plan to use our model to optimize combination drug regimens for TNBC in the future, our model reflects dynamics within the

TME from the time of a Stage II diagnosis to 168 days after. 168 days reflects current treatment protocols lasting 24 weeks for TNBC.⁹⁴ Each equation in the model begins with an input/source of a cell population and ends with an output/loss of that population, where each source or loss may be multiplied by one or several interactions. M2 macrophages have two loss terms, natural loss and polarization to M1 macrophages. For biological plausibility, we assume that every rate in our model has a finite bound. For example, the boosting effect of CAFs polarizing M1 macrophages to M2 macrophages (**arrow a**) must be limited; that is, it is not biologically plausible for CAFs to boost polarization without bound. This assumption is reflected in the boosting and inhibiting mechanisms, which we model with Michaelis-Menten terms to ensure that all rates remain bounded. We also assume that all cells in our model have finite lifespans.

Structural Identifiability and Model Reduction

The TME comprises numerous interacting cell types and signaling pathways, many of which exert overlapping and redundant effects. To maintain tractability and reduce structural identifiability challenges, we aggregated biologically-aligned mechanisms into single effective pathways. For example, M2 macrophage-mediated suppression of cytotoxic T lymphocytes occurs through multiple mechanisms, including immune checkpoint signaling, cytokine release, and metabolic competition. Rather than modeling each mechanism explicitly, we represented their combined net effect through a single inhibitory pathway. Similarly, the influence of M1 macrophages on T-cell activation is captured indirectly through polarization dynamics rather than as a separate cell population.

These modeling choices reflect a balance between biological realism and parameter identifiability. While individual parameters should not be interpreted independently in all cases, the model structure enables robust analysis of pathway-level influence on tumor dynamics. Future work incorporating additional information and data may allow further mechanistic resolution of these aggregated effects.

Equations

Equation (1): Pathway c represents the source of M2 macrophages recruited to the TME. This includes M1 macrophages that are polarized to M2 macrophages,⁹⁵ and undifferentiated monocytes that are directly polarized to M2 macrophages, which regularly occurs in cancer.^{95,96} We use **pathway l** to model that M2 macrophage recruitment is dependent on the existence of the TNBC tumor. Since we are modeling the TME of TNBC, we require that TNBC cells exist, in order to measure immune cells on or surrounding the tumor. We label the source of M2 macrophages as **pathway c,l** to reflect this dependency and we use a Michaelis-Menten term to model this process. We did not include a carrying capacity for M2 macrophages, as monocytes are continuously produced from the bone marrow. Instead, the M2 macrophage population is inherently bounded by the TNBC tumor's carrying capacity. This source is multiplied by **pathway a**, which represents the boost in the M2 macrophage population from CAFs polarizing M1 macrophages to M2 macrophages. We model the possible repolarization of M2 macrophages to M1 macrophages using **pathway e**, which is multiplied by **pathway h**, due to the boost that CTLs can have on this repolarization process.^{97,98} This is followed by the natural loss of M2 macrophages, with the rate constant δ_2 multiplied by M_2 to represent that M2 macrophages are lost in proportion to their population size.

Equation (2): CAFs are the most-abundant stromal cell in the TNBC microenvironment.⁹⁹ Tumor cells influence normal fibroblasts to differentiate to CAFs,¹⁰⁰ represented by **pathway d,m**. Since CAFs are resident fibroblasts that are activated, rather than recruited to the environment, we include a carrying

capacity term, $(1 - \frac{F}{K_F})$, to limit their growth. The other factors in this growth term represent a proportion of the TNBC cell level. **Pathway k** represents the death rate of CAFs.

Equation (3): The first term begins with proliferation of the breast cancer cells, represented by **j**, which we assume can be modeled by logistic growth.¹⁰¹ This is multiplied by the boosting effects from M2 macrophages (**arrow f**) and CAFs (**arrow g**).¹⁰² The loss term is multiplied by a boosting effect from CTLs directly killing tumor cells (**arrow t**).⁷⁵ There are multiple mechanisms that inhibit this CTL killing activity. We multiply by factors that represent M2 macrophages suppressing CTL activity (**arrow o**),¹⁰³ TNBC cells inactivating CTLs using PD-L1 (**arrow r**),¹⁰⁴ and Tregs suppressing CTLs (**arrow w**).⁸³

Equation (4): The first term begins with proliferation of CTLs, term **q**, which we assume can be modeled by logistic growth because they divide rapidly (but not without bound) via clonal expansion.¹⁰⁵ When M2 macrophages are repolarized into M1 macrophages, the resulting M1 macrophages will resume antigen presentation, resulting in CTL proliferation.¹⁰⁶ Since M1 macrophages are not explicitly represented in the model, we model this boost by multiplying α_{2C} by $\gamma_2 M_2$, the repolarization rate of M2 to M1. Therefore, we can write term **n** as

$$(1 + \frac{\alpha_{2C} \gamma_2 M_2}{\beta_{2C} + \gamma_2 M_2})$$

However, since γ_2 is a constant, we can divide the fraction by γ_2 and obtain:

$$(1 + \frac{\alpha_{2C} M_2}{\frac{\beta_{2C}}{\gamma_2} + M_2})$$

$$\frac{\beta_{2C}}{\gamma_2}$$

Since $\frac{\beta_{2C}}{\gamma_2}$ is still a constant, we absorb γ_2 into β_{2C} and call this whole quantity β_{2C} . Although M2 macrophages inhibit CTL proliferation,¹⁰⁷ we did not include this in the model, as it would cause an identifiability issue with **pathway o**. Instead, we use **pathway o** as a catch-all term for any inhibition M2 macrophages have on CTLs. The last term in this equation represents the natural loss of CTLs (**pathway v**).

Equation (5): The **t** terms represent the recruitment of Tregs. Terms **b** and **p** are the boosting effects that M2 macrophages and TNBC cells, respectively, have on Treg recruitment.^{42,108} This is followed by a natural loss term (**pathway x**).

Pathways

Label	Description	References
a	CAFs promote differentiation of monocytes to M2 macrophages and polarization of M1 to M2	4,43-47
b	M2 macrophages boost recruitment of Tregs	59,60
c	M0 macrophages differentiate into M2 macrophages, and M1 macrophages polarize to M2 macrophages	40,42
d	Normal fibroblasts are transformed into CAFs	65,66
e	M2 macrophages repolarize to M1 macrophages	62,63
f	M2 macrophages promote proliferation of tumor cells	4,46

g	CAFs promote proliferation of tumor cells	68
h	CTLs promote M2 polarization to M1	79
i	M2 macrophages naturally die	109
j	Breast cancer cells proliferate	110,111
k	CAFs naturally die	112
l	Tumor cells induce M1 polarization to M2	4,38,48
m	Tumor cells cause normal fibroblasts to differentiate into CAFs	67,68
n	M2 to M1 polarization boosts proliferation of CTLs	77
o	M2 macrophages suppress CTL activity	49–52
p	Tumor cells promote Treg recruitment	86–88,113
q	CTLs proliferate	80
r	Tumor cells inactivate CTLs	76
s	Tregs are recruited	80
t	CTLs kill tumor cells	75
u	Breast cancer cells naturally die	114
v	CTLs naturally die	80
w	Tregs suppress CTL cytotoxic function	90
x	Tregs naturally die	80
y	Tregs inhibit CTL proliferation	91,92

Table 1. Description of pathways included in Fig 1.

Initial Value Calculations

Initial conditions were selected to represent approximate average magnitudes of immune and stromal cell populations within a Stage II TNBC tumor rather than precise patient-specific values. Because quantitative measurements of absolute immune cell densities in human TNBC tumors are limited and heterogeneous, we combined estimates from single-cell transcriptomics, histopathological studies, tumor geometry, and reported cell size ranges to generate biologically plausible starting values. These initial conditions are intended to establish reasonable baseline scales for simulation rather than exact biological measurements.

We used analysis results from the single cell transcriptomics article by Guo et. al, specifically Figure 8A, to estimate the immune cell compositions within TNBC tumor samples.¹¹⁵ We estimated an

average cell proportion of 10% CD8+ T cells, 4% Tregs, and 12% M2 macrophages. CAFs were not included in this study, so we use the fact that Sun et al. measured a median percentage of α -SMA-positive stroma cells to be 69%.¹¹⁶ “Stroma-intermediate primary breast carcinoma” is quantified as 50% stroma.¹¹⁷ Therefore, we estimated the percentage of a TNBC tumor to be $(.69)(.5) = 34.5\%$ CAFs. To calculate relative densities of immune cells within a Stage II TNBC tumor, we used the fact that Stage II tumors are diagnosed beginning at a size of 2 cm,¹¹⁸ where 2 cm represents the longest diameter of the tumor. Since many breast cancers tend to be discoidal,¹¹⁹ we used an ellipsoid formula to estimate the volume of a Stage II tumor to be $(4/3)(\pi)(1)(1)(0.5) = 2.0944 \approx 2.09 \text{ cm}^3$ assuming the shorter diameter is half the length of the longest. For each cell type, we took a percentage of this volume, and then converted from volume to density using the mass of each cell type.

Limitations of these initial value calculations include the fact that the analysis performed on only ten tumor samples, that Guo et al. did not report the stage of each TNBC tumor, and that two TNBC patients had been treated before. Therefore these initial values are an estimate of average magnitude rather than an exact report of immune cell composition. Additionally, TNBC tumors are known to be heterogeneous, so initial values of immune cells, even at a collective “Stage 2” timeline, certainly vary by patient. After calculating a starting estimate using the process outlined above, we tweaked our initial values using our own clinical expertise.

M_{20} : M2 macrophages are 12% of total tumor volume, implying 0.251328 cm^3 of the initial tumor volume is M2 macrophages. Monocytes can have a diameter up to 22 microns,¹²⁰ which is equivalent to 0.0022 centimeters. Since monocytes are typically spherical, we estimate their volume to be $5.57528\text{e-}9$ (where the scientific notation of e-9 is used to mean $\times 10^{-9}$) cm^3 using a spherical volume formula, so that the total number of M2 macrophages within the tumor is $0.251328 \text{ cm}^3 / 5.57528\text{e-}9 = 45078991.5484$. To get an average density, we assume the M2 macrophages are uniformly distributed throughout the tumor, so we calculate $45078991.5484 / 2.0944 \text{ cm}^3 = 21523582.6721 / \text{cm}^3$, or approximately 21500 cells/mm³ as a starting estimate. This initial value was not subsequently adjusted.

F_0 : CAFs are 34.5% of total tumor volume, implying 0.722568 cm^3 of the initial tumor volume is CAFs. Since CAFs in our model are measured as total volume, we took 34.5% of initial tumor volume, so $0.345 * 2.0944 = 0.722568 \text{ cm}^3$ or approximately 722 mm³ as a starting estimate for the initial volume of CAFs. This initial value was not subsequently adjusted.

B_0 : Since Stage II tumors are diagnosed starting at a longest diameter of 2 cm, and as mentioned previously, most tumors are discoidal, we calculate an initial tumor volume of

$$\frac{4}{3}\pi(1)(1)(0.5) = 2.0944 \approx 2.09 \text{ cm}^3, \text{ or } 2090 \text{ mm}^3. \text{ This value was not subsequently adjusted.}$$

T_{C0} : CTLs are 10% of total tumor volume, implying 0.20944 cm^3 of the initial tumor volume is comprised of CTLs. T lymphocytes have an average diameter of 9.5 microns,¹²¹ which is equivalent to 0.00095 centimeters. Since T lymphocytes are spherical, we estimate their volume to be $4.4892\text{e-}10 \text{ cm}^3$ so that the total number of CTLs within the tumor is $0.20944 \text{ cm}^3 / 4.4892\text{e-}10 \text{ cm}^3 = 4.66541922837\text{e}8$. To get an average density, we assume the CTLs are uniformly distributed throughout the tumor, so we calculate $4.66541922837\text{e}8 / 2.0944 \text{ cm}^3 = 2.22756838635\text{e}8 / \text{cm}^3$, or $2.22756838635\text{e}8 / \text{mm}^3$. The 10% statistic was taken from Guo et al.’s measurement of CD8+ T cells within TNBC tumors, which may not reflect the proportion of active CTLs within TNBC tumors, which is likely less. We estimated 60% of these CD8+ T cells may be active, for an initial value of $0.60 * 2.22756838635\text{e}8 = 133654.103181$ or approximately 134,000.

T_{R_0} : Tregs are 4% of total tumor volume, implying 0.083776 cm³ of the initial tumor volume is Tregs. We assume that Tregs, like CTLs, have an average diameter of 9.5 microns,¹²¹ which is equivalent to 0.00095 centimeters. Since T lymphocytes are spherical, we estimate their volume to be 4.4892e-10 cm³ so that the total number of Tregs within the tumor is 0.083776 cm³/4.4892e-10 cm³ = 1.86616769135e8. To get an average density, we assume the Tregs are uniformly distributed throughout the tumor, so we calculate 1.86616769135e8/2.0944mm³ = 8.9102735454e7. We adjusted this value to 10.9e3 based on our clinical authors' input.

Initial Values			
Cell	Value	Units	References
M_2	21500	cells/mm ³	115,120
F	722	mm ³	116,117
B	2090	mm ³	118,119
T_C	134000	cells/mm ³	115,121
T_R	10900	cells/mm ³	115,121

Table 2. Initial values used in simulations of our model.

We emphasize that TNBC tumors are highly heterogenous, and immune cell infiltration varies substantially between patients. Accordingly, these initial values should be interpreted as representative averages. After deriving initial estimates using the procedures described above, values were adjusted when necessary based on clinical expertise to ensure biological plausibility. The qualitative behavior of the model is not intended to depend on exact initial values but rather on the structure of interactions and relative strengths of modeled pathways.

Parameter Calculations

To calculate the alpha parameters, we searched for experimental data that yielded the rates of growth of a population with and without the effect of interest in the context of TNBC. Then, we could take a ratio of these rates, to find a fold increase or decrease, depending on the parameter. We systematically estimated beta parameters by taking the corresponding cell population's initial value and

multiplying it by 4. For proliferation rates, we found doubling times and used the formula $p = \frac{\ln 2}{d}$ where p is proliferation rate and d is doubling time. For loss rates, we found average half-life estimates (

$$\delta = \frac{\ln 2}{t_{\frac{1}{2}}}$$

) and used $\delta = \frac{\ln 2}{t_{\frac{1}{2}}}$. Carrying capacities were estimated as a fraction of total tumor carrying capacity, which was found through literature, and then converted to appropriate units. Recruitment rates and polarization rates were estimated from literature when possible and estimated by clinical authors' input when not. Parameters that were not calculable with literature are labeled as "estimated", to represent the estimation from clinical authors' expertise. For some parameters, we only had access to data in a setting

other than TNBC. A future endeavor related to this work is gathering data to parameterize our model in the TNBC setting. Further limitations are detailed in the Discussions section.

Alpha Parameters

Recall α_{XY} represents a maximum boost or inhibition that cell population X can have on a mechanism from cell population Y . When possible, we calculated each α_{XY} by using experimental results that documented both the efficacy of the mechanism from Y alone and the efficacy of the mechanism from Y with the presence of X . A ratio of these efficacies represents α_{XY} , the efficacy fold increase or

decrease due to population X . Because each boosting and inhibition term looks like $(1 \pm \frac{\alpha_{XY}X}{\beta_{XY} + X})$, $(1 \pm \alpha_{XY})$ is the limit of this term as X gets larger and larger, so in fact $(1 \pm \alpha_{XY})$ is the maximum boost or inhibition, and thus in a boosting case, α_{XY} is obtained by taking the ratio of efficacies and subtracting 1. In an inhibition case, α_{XY} is obtained by subtracting the ratio of efficacies from 1. These conventions are used throughout the parameter calculations section.

α_{B2} : Leonard et al. measured macrophage migration toward mouse model breast cancer cells in a migration chamber.¹²² We used Figure 2b in their article to estimate that 200 macrophages, as noted by the conditioned 4T1 medium column of the control, migrated toward tumor cells over a 48 hour period. Assuming a linear migration rate, this amounts to 100 macrophages per day. This study used 8000-10000 breast cancer tumor cells, so we estimate the recruitment rate in our model to be higher, due to the number of breast cancer cells in our setting being orders of magnitude higher. We therefore estimated α_{B2} to be 10,000 macrophages per day.

α_{F2} : Cohen et al. studied how Chi3L1 recruits macrophages and how it induces an M2-like phenotype in breast cancer.⁴³ Figure 4L in Cohen's study shows the fold change of the ratio of CD206/CD86 expression between macrophages mixed with recombinant Chi3L1 and serum-free macrophages (SFM). We estimated the fold change to be 2.2 from this diagram, resulting in $\alpha_{F2} = 2.2 - 1 = 1.2$.

α_{C2} : Sharma et al. studied mechanistic interactions between intratumoral effector T cells and tumor-associated macrophages.⁷⁹ The authors show CTL activity can be restored with a combination of anti-CTLA-4 and a vaccine that activates the ICOS pathway (IVAX). Since α_{C2} represents the maximum effect CTLs can have on repolarizing M2 macrophages to M1 macrophages, we use their control setting (quantified by the black control bar in Figure S3D of Sharma et al.) to estimate the efficacy of M2 repolarizing to M1 in absence of CTLs, and their setting with anti-CTLA-4 and IVAX treatment (quantified by the blue bar in Figure S3D of Sharma et al.) to estimate the efficacy of repolarization in the presence of CTLs. We estimate the black bar (control) in Figure S3D in Sharma et al. to be 48% and the blue bar (anti-CTLA-4 + IVAX) to be 12%,⁷⁹ giving us a fold change of $0.48/0.12 = 4$. Thus, $\alpha_{C2} = 4 - 1 = 3$.

α_{2B} : Tu et al. studied how M2 macrophages contribute to breast cancer cell proliferation.¹²³ We used Figure 1B in Tu's study to calculate the maximum boosting effect M2 macrophages can have on triple-negative breast cancer cell proliferation. Because we are estimating the maximum effect, we chose to use the timepoint of 48 hours, when the difference between the proliferation rate in the control (black line) and the proliferation rate in the setting with the supernatant medium of M2 macrophages (blue line) is the largest. We took $2.9/2.2$ as the ratio of proliferation of breast cancer cells with M2 macrophages to proliferation of breast cancer cells with no macrophages to get 1.318. Thus, $\alpha_{2B} = 1.318 - 1 = 0.318$.

α_{FB} : Takai et al. studied CAFs in human TNBC and how they promote tumor growth.⁶⁶ We used Figure 2B to approximate the fold change of tumor growth in the presence CAFs versus tumor growth in the

absence CAFs, assuming the loss of TNBC is negligible in each setting. We take the widest gap, at day 25, and estimate the tumor volume with CAFs (gray curve) to be 2100 mm^3 , and estimate the tumor volume without CAFs (black curve) to be 800 mm^3 , which yields a fold change of $2100/800 = 2.625$. Thus $\alpha_{FB} = 2.625 - 1 = 1.625$, or approximately 1.63.

α_{CB} : Khazen et al. studied how CTL population density can affect controlling tumor killing efficacy in melanoma tumors.¹²⁴ We used Figure 5 in their study to estimate the maximum cytotoxic effect CTLs can have on breast cancer tumor cells. We used the widest gap, at day 7, to estimate a fold change of tumor size with no injections of CTLs versus tumor size with 3 injections of CTLs. At day 7, we estimate the tumor size with no injections (black curve) to be 150 mm^3 , and the tumor size with 3 injections (green curve) to be 5 mm^3 . Then to obtain a fold change, we take $150/5 = 30$, so $\alpha_{CB} = 30 - 1 = 29$.

α_{2CB} : Mercier et al. studied the V-domain Ig suppressor of T-cell activation (VISTA) checkpoint in mice with melanoma.⁹⁸ Figure 1A in their article shows tumor growth in a control population and tumor growth in a population treated with 13F3, a VISTA inhibitor. Because the VISTA inhibitor will inhibit M2 macrophage polarization,¹²⁵ we consider the black curve (control) to represent tumor growth where M2 macrophages are present, inhibiting CTL activity maximally. We consider the red curve (13F3) to represent tumor growth without any M2 inhibition of CTLs killing tumor cells. Thus, to calculate the maximum potential suppressive activity of M2 on CTLs, we chose to take the widest gap between the black and red curves, at Day 18. We estimated the untreated tumor size at Day 18 to be 91 mm^2 and the 13F3 treated tumor size at Day 18 to be 22 mm^2 . Therefore, we calculated the ratio of CTL killing of tumor cells with no M2 inhibition of CTLs to maximal M2 inhibition of CTL killing of tumor cells to be $22/91 = 0.24175824175$. The number 0.24175824175 corresponds to the maximum inhibitory effect M2 macrophages can have on CTLs, so to reflect this in the model we take $\alpha_{2CB} = 1 - 0.24175824175 = 0.75824175825 \approx 0.758$.

α_{BCB} :

$$\underbrace{\left(1 + \frac{\alpha_{CB} T_C}{\beta_{CB} + T_C}\right)}_{\text{t}} \underbrace{\left(1 - \frac{\alpha_{2CB} M_2}{\beta_{2CB} + M_2}\right)}_{\text{o}} \underbrace{\left(1 - \frac{\alpha_{BCB} B}{\beta_{BCB} + B}\right)}_{\text{r}} \dots$$

At the end of Equation (3), the factors represent the combined effects of **pathways t, o, and r** on the death of breast cancer cells. Shi et al. found the average percent of CD8+ T cells producing granzyme in healthy donors, which we use as a proxy to measure cytotoxic activity, to be approximately 30% in Figure 1G,¹²⁶ and Abudula et al. showed in Figure 5F that the percent of CD8+ T cells producing granzyme under the suppressive effects of tumor cells and macrophages is approximately to be 1.3%.¹²⁷ This implies the total reduction effect of both tumor cells and macrophages combined can be estimated by a fold change of $0.013/0.3 = 0.0433$. If we assume this is the largest possible suppression, then we have

$$\underbrace{\left(1 - \alpha_{2CB}\right)}_{\text{o}} \underbrace{\left(1 - \alpha_{BCB}\right)}_{\text{r}} = 0.0433$$

and since we have

$$\underbrace{\left(1 - \alpha_{2CB}\right)}_{\text{o}} = 0.24175824175$$

(see α_{2CB}), then

$$\underbrace{\left(1 - \alpha_{BCB}\right)}_{\text{r}} = 0.043/0.24175824175 = 0.17786363637,$$

and

$$\alpha_{BCB} = 1 - 0.17786363637 = 0.82213636363 \approx 0.822.$$

α_{RCB} : Chen et al. studied how Tregs can suppress CTL cytotoxicity through TGF- β in vivo.¹²⁸ We used Figure 4b to estimate about 55% of naive CD8 cells are capable of lysis versus 25% of CD8 cells are capable of lysis when they are co-cultured with Tregs. Therefore we calculate the fold change of CTL activity without Tregs versus CTL activity with Tregs to be $0.25/0.55 = 0.455$, so

$$\alpha_{RCB} = 1 - 0.455 = 0.545.$$

α_{2C} : The α_{2C} parameter is used to represent the maximum boosting effect M1 macrophages, modeled by the loss of M2 macrophages, can have on CTL proliferation. Kaneda et al. show that a PI3K γ inhibitor can repolarize TAMs from M2 to M1 in breast cancer.¹²⁹ Using Figure 3c, we estimated a fold change of CD8+ T cells' ability to proliferate in the presence of macrophages with PI3K (green triangles) versus without PI3K (dark blue circles) to be $80/10 = 8$. Therefore, $\alpha_{2C} = 8 - 1 = 7$.

α_{RC} : Feinerman et al. studied regulatory T cells, effector T cells, IL-2, and interactions among these.¹³⁰ We use the IL-2 concentration measured in Figure 6b as a proxy for CTL proliferation potential. We estimated that at 61 hours the concentration of IL-2 in a setting with weak effector T cells in the presence of Tregs was 1.35 pM, compared to the concentration of IL-2 in a setting with weak effector T cells in the absence of Tregs, which we estimated to be 25 pM. Thus, the fold decrease in IL-2 due to the presence of Tregs is $\frac{1.35}{25} = 0.054$, so the maximum inhibition Tregs can have on CTL proliferation is $1 - 0.054 = 0.946$.

α_{2R} : Semba et al. studied JNK-active TNBC clusters in the TNBC TME.¹³¹ They found JNK promotes an immunosuppressive TME via macrophage-derived CCL2. 80% of the CCL2 expressing cells are TAMs. Therefore, in Figure 1c, we assume the difference between the estimated fraction of Tregs in pJNK-low tumors and pJNK-high tumors is due to M2 macrophages. The estimated fraction of Tregs in pJNK-high tumors is 2.5, and the estimated fraction of Tregs in pJNK-low tumors is 1.7. Therefore, we estimate the fold change of Treg recruitment in the presence of M2 macrophages versus in the absence M2 macrophages to be $2.5/1.7 = 1.47058823529$, so

$$\alpha_{2R} = 1.47058823529 - 1 = 0.47058823529 \approx 0.471.$$

α_{BR} : Zahran et al. studied the accumulation of Tregs in TNBC.⁸³ We calculated the maximum boosting effect TNBC can have on recruiting Tregs using Table 2. The authors found 6.6% of malignant tissue was CD4+CD25+highFoxP3+Tregs versus 3.2% in normal tissue. We can use these percentages to calculate a $0.066/0.032 = 2.0625$ fold change between Treg recruitment in the presence of TNBC versus homeostatic Treg recruitment in normal tissue. Therefore, $\alpha_{BR} = 2.0625 - 1 = 1.0625 \approx 1.063$.

Beta Parameters

β_{2C} : We calculated β_{2C} by taking $4 \times M_{20}$, we then divided by $\gamma_2 = 0.005$, to get our final estimate of 17,200,000 cells per mm³.

β_{2X} : For all other betas associated with M2 macrophages, we calculated $4 \times M_{20} = 4 * 21500 = 86000$ cells per mm³.

β_{FX} : For any beta associated with CAFs, we calculated $4 \times F_0 = 4 * 722 = 2888 \approx 2890$.

β_{BX} : For any beta associated with TNBC cells, we calculated $4 \times B_0 = 4 * 2090 = 8360 \text{ mm}^3$.

β_{CX} : For any beta associated with CTLs, we calculated $4 \times T_{C0} = 4 * 111000 = 444000$.

β_{RX} : For any beta associated with Tregs, we calculated $4 \times T_{R0} = 4 * 10900 = 43600$.

Carrying Capacities

K_F : As detailed in the initial values calculations, we estimated 34.5% of an average TNBC tumor is CAFs. To ensure the carrying capacity would bound tumors of varying sizes, K_F was taken to be 50% of K_B . Hence, $K_F = 0.5 * 262 = 131 \text{ cm}^3$ or 131000 mm^3 .

K_B : was calculated using data from a study by Chen et al. that found a TNBC tumor with a 10 cm diameter.¹³² Since breast cancer tumors tend to be discoidal,¹¹⁹ we estimated the maximum volume of a TNBC tumor to be

$$K_B = \frac{4}{3}\pi(5)(5)(2.5) = 261.79939 \approx 262 \text{ cm}^3,$$

where 5 is the radius of the longer directions and 2.5 is the radius of the shorter one. This is equivalent to 262000 mm^3 .

K_C : Using the fact that $K_B = 262000 \text{ mm}^3$, and that CTLs make up roughly 10% of a TNBC tumor, about 26200 mm^3 can contain T_C . As calculated in the initial value section, T_C have an estimated volume to be $4.489 \times 10^{-10} \text{ cm}^3$, or $4.489 \times 10^{-7} \text{ mm}^3$. This means $26200 / (4.489 \times 10^{-7}) = 58364891958.1$ total T_C can fit in that large of a tumor. Dividing by 262000 mm^3 (130900) again yields $222766.763199 \text{ cells/mm}^3$ or approximately 223,000 cells/mm³ for K_C .

Source and Proliferation Parameters

σ_F : Longitudinal data on differentiation rates of normal fibroblasts to CAFs is limited. We assume that CAF differentiation is slower relative to tumor cell proliferation.¹³³ To reflect this assumption, we estimated $\sigma_F = 0.1p_B = 0.000998$.

p_B : was calculated using a study by Lee et al. that found a specific growth rate average of 1.003% per day in a group of 57 patients with triple-negative breast cancer.¹¹⁰ To convert this to a 1/day rate constant, we use an exponential growth formula

$$1.01003 = e^{p_B}$$

so we have $p_B = 0.00998$.

p_C : de Boer et al. (Table III) found a doubling time of CD8+ T cells during the expansion phase to be 8 hours, or $\frac{1}{3}$ days by fitting a model to data from mice infected with lymphocytic choriomeningitis virus.¹³⁴ Using their raw data to convert this to a proliferation rate, we use

$$p_C = \frac{\ln 2}{0.33} = 2.08.$$

σ_R : Shanahan et al. studied Treg recruitment in a murine model of lung cancer.¹³⁵ Using Figure 5A, we estimated 6700 Tregs were recruited to the lung of a tumor-bearing mouse in 16 hours, or 2/3 days. We estimated that a mouse's lung has a total volume of 1 milliliter,¹³⁶ and we used Figure 5G to estimate 1.85% of the total lung is tumor. This implies that $1000\mu\text{L} \times 0.0185 = 18.5\mu\text{L}$ is the total volume of the tumor used in the control of figure 5. We calculate a source rate as follows:

$$\frac{6700}{(18.5)\left(\frac{2}{3}\right)} = 543.2433 \approx 543$$

Loss Parameters

δ_2 : was estimated using Eftimie and Barelle's model of immune responses in lung cancer that was parameterized with murine data.¹³⁷ The natural death rate of macrophages fell in a range between 0.09 and 0.14, and we chose 0.1155, the midpoint of this range.

δ_F : Weissman-Shomer and Fry found an average lifespan of chick embryo fibroblasts to be 57 days.¹³⁸ We believe CAFs to have a longer lifespan, so we took 0.1 times 1/57, which gives 0.00175.

δ_B : Mahacek et al. showed that a human breast cancer cell line isolated from a metastatic lymph node sample lived 200 days in vitro.¹¹⁴ We assumed this to be an upper bound on the lifespan of primary triple-negative breast cancer cells due to their aggression. A lifespan of 200 days give an upper bound for the death rate constant of $1/200 = 0.005$; we estimate an order of magnitude less so that $\delta_B = 0.0005$.

δ_C : de Boer et al. found a half-life of 41 hours for activated CD8+ T cells.¹³⁴ We converted this to an average death rate by dividing $\ln(2)$ by half-life, so we calculate

$$\delta_C = \frac{\ln 2}{\frac{41}{24}} = 0.406$$

δ_R : Vukmanovic-Stejic et al. used deuterium labeling to monitor disappearance of Tregs in healthy volunteers.⁸⁴ The authors found that Tregs have a half-life of about 11 days, which yields an average death rate constant of $\delta_R = 0.0630$.

Repolarization and Proportionality Parameters

γ_2 : Xiao et al. induced M2 to M1 repolarization using targeted codelivery of STAT6 inhibitor and IKK β siRNA to mice in a subcutaneous breast cancer model.⁹⁷ Mice in the control group (treated only with phosphate-buffered saline) had 1.81% of total tissue as M2-like TAMs on Day 8, whereas mice treated with combination therapy group (ST-AS&Si) had 0.33%. We assumed that ST-AS&Si treatment causes

more M_2 to M_1 polarization than usual. Thus we used $\frac{0.0033}{0.0181} \approx 0.1823$ as the lower bound for the fold change of number of M2 macrophages between a treated and untreated setting., where we assume the treated setting results in fewer macrophages due to M2 to M1 repolarization. In our differential equation,

rate of change of M_2 , the expression $-\gamma_2 M_2$ represents the rate of M_2 to M_1 polarization. is of the form Thus we used the following exponential decay formula to calculate an upper bound for γ_2 :

$$e^{-8\gamma_2} = 0.1823$$

where 8 is chosen because macrophages were measured on Day 8. Solving for γ_2 gives 0.2128 an upper bound for the basal M2 to M1 repolarization rate. We felt 0.005 was reasonable as this basal rate.

Parameters							
#	Symbol	Description	Label	Value	Units	Sources	Setting
1	α_{B2}	Maximum source rate of M2 macrophages	c,l	10000	cells/mm ³ *day	¹²²	Murine model of TNBC
2	β_{B2}	Threshold for half of maximum effect of TNBC cells on M1 to M2 polarization	c,l	8360	mm ³	estimated	
3	α_{F2}	Maximum fold change boost in M1 to M2 polarization due to CAFs	a	1.2	unitless	⁴³	Murine model of breast cancer
4	β_{F2}	Threshold for half of maximum fold change boost in M1 to M2 polarization due to CAFs	a	2890	mm ³	estimated	
5	γ_2	M2 to M1 polarization rate constant	e	0.005	1/day	⁹⁷	Murine model of TNBC
6	α_{C2}	Maximum boosting effect by CTLs on M2 to M1 polarization	h	3	unitless	⁷⁹	Murine model of melanoma
7	β_{C2}	Threshold for half of maximum boosting effect by CTLs on M2 to M1 polarization	h	536000	cells/mm ³ *day	estimated	
8	δ_2	M2 loss rate constant	i	0.116	1/day	¹³⁷	Non-small cell lung cancer mathematical model parameterized with murine data
9	σ_F	CAF source rate constant	d,m	0.000998	1/day	estimated	

10	K_F	CAF carrying capacity	d,m	65450	mm ³	¹³⁹	Human patients with breast cancer (multiple subtypes)
11	δ_F	CAF loss rate constant	k	0.00175	1/day	¹³⁸	Normal fibroblasts in chick embryos
12	p_B	TNBC cell proliferation rate constant	j	0.00998	1/day	¹¹⁰	Human patients with TNBC
13	K_B	TNBC cell carrying capacity	j	262000	mm ³	^{119,132}	Human patients with TNBC
14	α_{2B}	Maximum boost by M2 macrophages on TNBC cell proliferation	f	0.318	unitless	¹²³	Human patients with TNBC
15	β_{2B}	Threshold for half of the maximum boost by M2 macrophages on TNBC cell proliferation	f	86000	cells/mm ³	estimated	
16	α_{FB}	Maximum boost by CAFs on TNBC cell proliferation.	g	1.63	unitless	⁶⁶	Murine xenograft model of TNBC
17	β_{FB}	Threshold for half of the maximum boost by CAFs on TNBC cell proliferation	g	2890	mm ³	estimated	
18	δ_B	TNBC cell loss rate constant	u	0.0005	1/day	¹¹⁴	Human patients with TNBC
19	α_{CB}	Maximum cytotoxic effect CTLs have on TNBC cells.	t	29	unitless	¹²⁴	Murine model of melanoma
20	β_{CB}	Threshold for half of the maximum cytotoxic effect CTLs	t	536000	cells/mm ³	estimated	

		have on TNBC cells.					
21	α_{2CB}	Maximum inhibition effect M2 macrophages have on CTL cytotoxic activity	o	0.758	unitless	⁹⁸	Murine model of melanoma
22	β_{2CB}	Threshold for half of the maximum inhibition effect M2 macrophages have on CTL cytotoxic activity	o	86000	cells/ mm ³	estimated	
23	α_{BCB}	Maximum inhibition effect TNBC cells have on CTL cytotoxic activity	r	0.822	unitless	^{126,127}	Healthy human subjects; murine model of TNBC
24	β_{BCB}	Threshold for half of the maximum inhibition effect TNBC cells have on CTL cytotoxic activity.	r	8360	mm ³	estimated	
25	α_{RCB}	Maximum suppressive effect Tregs have on CTL cytotoxic activity.	w	0.545	unitless	¹²⁸	Murine model of colon carcinoma
26	β_{RCB}	Threshold for half of the maximum inhibition effect Tregs have on CTL cytotoxic activity.	w	43600	cells / mm ³	estimated	
27	p_C	CTL proliferation rate	q	2.08	1/day	¹³⁴	Murine model of acute lymphocytic choriomeningitis
28	K_C	CTL carrying capacity	q	223000	cells/mm ³	estimated	

29	α_{2C}	Maximum boost by M1 macrophages on CTL proliferation	n	7	unitless	¹²⁹	Murine model of various cancers
30	β_{2C}	Threshold for half of the maximum boost by M1 macrophages on CTL proliferation	n	17200000	cells/mm ³	estimated	
31	α_{RC}	Maximum inhibition Tregshave on CTL proliferation	y	0.946	unitless	¹³⁰	In vitro studies of cells from healthy murine subjects
32	β_{RC}	Threshold for maximum inhibition Tregs have on CTL proliferation	y	43600	cells/mm ³	estimated	
33	δ_C	CTL death rate constant	v	0.406	1/day	¹³⁴	Murine model of acute lymphocytic choriomeningitis
34	σ_R	Treg recruitment rate	s	583.33	cells/mm ³ *day	¹³⁵	Murine model of lung cancer
35	α_{2R}	Maximum boost by M2 macrophages on Treg recruitment.	b	0.471	unitless	¹³¹	Murine model of TNBC
36	β_{2R}	Threshold for the boost by M2 macrophages on Treg recruitment.	b	86000	cells/mm ³	estimated	
37	α_{BR}	Maximum recruitment effect TNBC cells have on Tregs.	p	1.063	unitless	⁸³	Human patients with TNBC
38	β_{BR}	Threshold for half of the maximum boost	p	8360	mm ³	estimated	

		by TNBC cells have on Treg recruitment					
39	δ_R	Treg loss rate constant	x	0.0630	1/day	84	Healthy human subjects

Table 3. Parameter Descriptions and Nominal Values

Parameter definitions, nominal values, units, data sources, and experimental or clinical settings used to parameterize the model.

Simulations and Sensitivity Analysis

Our simulations provide predictions for the dynamics of the TME of a TNBC tumor. All cell populations increase over time. CTLs increase and rapidly approach a low steady-state value. Within 250 days, immune cells within an untreated TNBC tumor will reach their steady-states, with CAFs still growing in number, contributing to metastasis and epithelial-to-mesenchymal transition.¹⁴⁰ By day 500, in our model an untreated Stage II TNBC tumor is predicted to reach its carrying capacity.

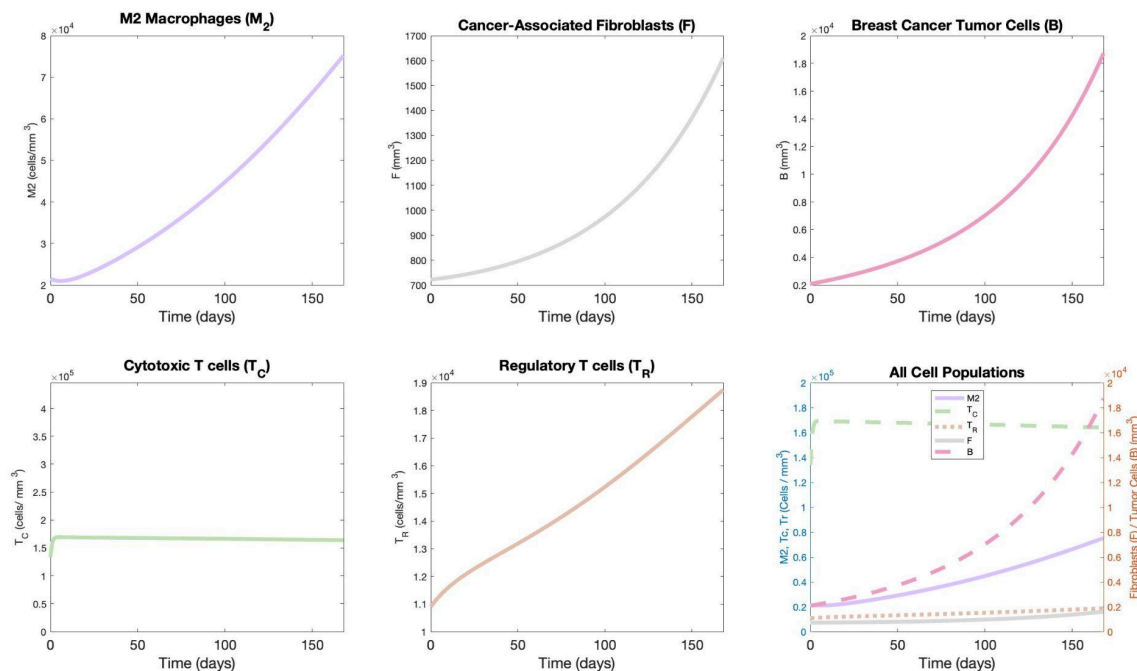


Figure 2. Simulations of tumor and immune cell populations over a 168 day period.

Caption:

Plots created with ode45 function in MATLAB R2024b to solve our system of differential equations using our nominal parameter values and initial values. Simulations of the cell populations over 168 days, a typical treatment period. Each population is plotted in a color matching its symbol on our model diagram (M2 in solid lavender, CAFs in solid gray, TNBC in solid pink, CTLs in dotted green, Tregs in dotted orange. The bottom right plot shows all cell populations together, where the left axis is in units of cells per mm³ (for M2, CTLs, and Tregs) and the right axis is in units of mm³ (for CAFs and TNBC cells).

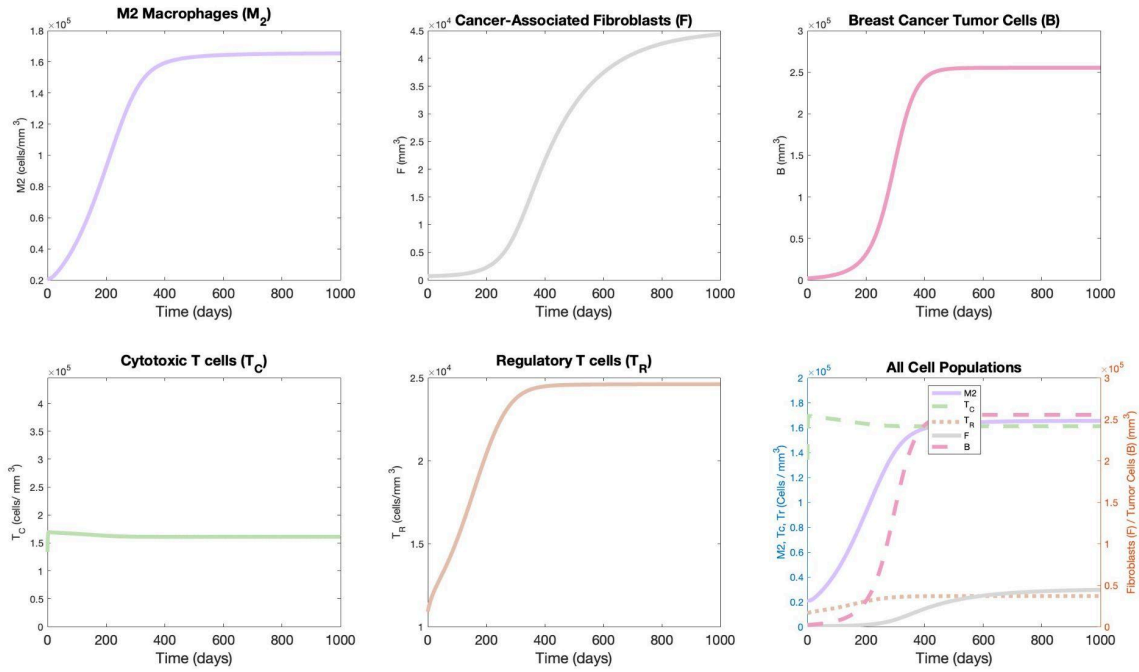


Figure 3. Simulations of tumor and immune cell populations over a 1000 day period. Caption: The same plot as Fig. 2, but with a timeframe of 1000 days to show longer-term behavior of each cell population in our model. Plots created with `ode45` function in MATLAB R2024b to solve our system of differential equations using our nominal parameter values and initial values. Simulations of the cell populations over 1000 days. Each population is plotted in a color matching its symbol on our model diagram (M2 in solid lavender, CAFs in solid gray, TNBC in solid pink, CTLs in dotted green, Tregs in dotted orange). The bottom right plot shows all cell populations together, where the left axis is in units of cells per mm^3 (for M2, CTLs, and Tregs) and the right axis is in units of mm^3 (for CAFs and TNBC cells).

We performed a global variance-based sensitivity analysis using the Sobol method.^{141,142} Our model has 39 parameters. Each parameter was allotted a uniform distribution, with its range bounded below by half its nominal value, and bounded above by 1.5 times its nominal value when possible. There were three exceptions, the inhibitory alpha parameters α_{2CB} , α_{BCB} , and α_{RC} which each have a nominal value larger than 2/3. Multiplying their nominal values by 3/2 would result in a number above 1, which would reverse the sign in these pathways. Thus, those two parameters were restricted to have an upper bound of 1. We used 175,000 base samples, which resulted in $(39+2)*(175,000) = 7,175,000$ model evaluations. Performing this type of sensitivity analysis determines the relative influence that the model parameters have on a specified quantity-of-interest (QoI). Our QoI is the volume of the TNBC tumor on Day 168, the end of a typical TNBC chemoimmunotherapy treatment period of 24 weeks.⁹⁴ We chose this QoI because we plan to use our model to compare clinical treatment regimens in silico in the future, and we wanted to determine which parameters influence the tumor size in a clinically-relevant timeframe and without any treatment, to establish a baseline. In descending order, the top six most-influential parameters in our model are the proliferation rate of TNBC cells, p_B , the maximum boosting effect CAFs have on TNBC proliferation, α_{FB} , the threshold for half of the maximum boosting effect CAFs have on TNBC proliferation, β_{FB} , the carrying capacity of the TNBC tumor, K_B , and the maximum boosting effect M2 macrophages have on TNBC proliferation α_{2B} .

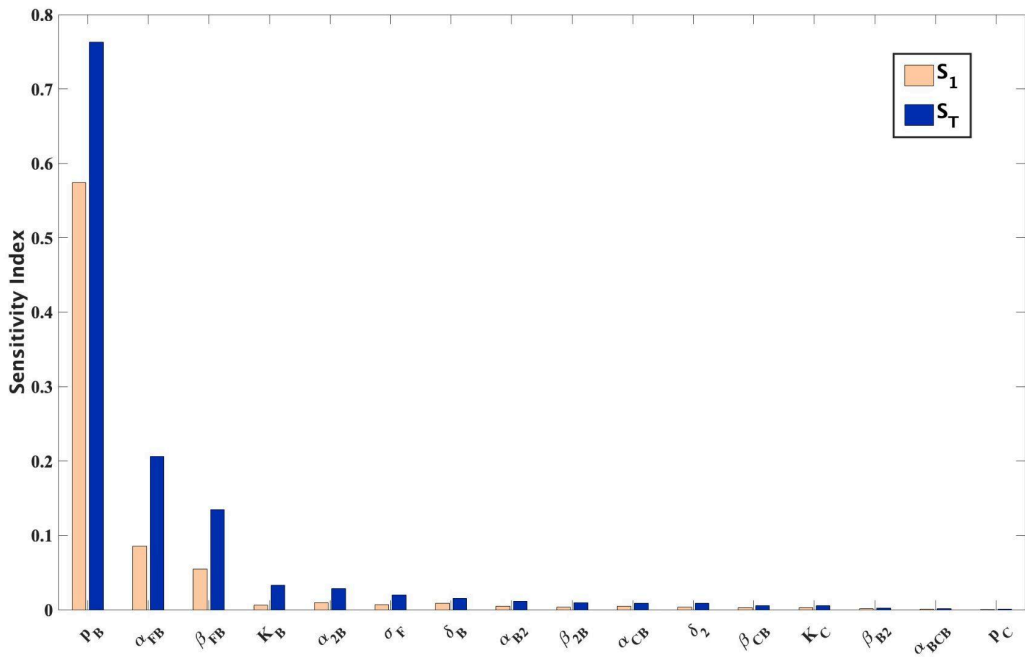


Figure 4. Global sensitivity analysis bar chart of TNBC tumor size at day 168.

Caption: We used MATLAB R2024b to perform a global sensitivity analysis on our model. Bar chart of the top 16 most-influential parameters on the size of the TNBC tumor on Day 168, in descending order of total-order Sobol sensitivity index, S_T . Parameters not shown have a total sensitivity index less than 9e-4. The height of each blue bar is the value of the Sobol total-order sensitivity index, S_T , and the height of each orange bar is the value of the Sobol first-order sensitivity index, S_1 .

The dominance of tumor-intrinsic parameters, such as TNBC proliferation rate and tumor carrying capacity, is expected given their direct role in managing tumor growth. Importantly, beyond these intrinsic factors, the sensitivity analysis reveals that stromal- and immune-mediated pathways, particularly CAF-driven tumor support and M2 macrophage driven tumor support, are among the most influential contributors to tumor burden. These findings suggest that modulation of the TME may substantially impact disease progression.

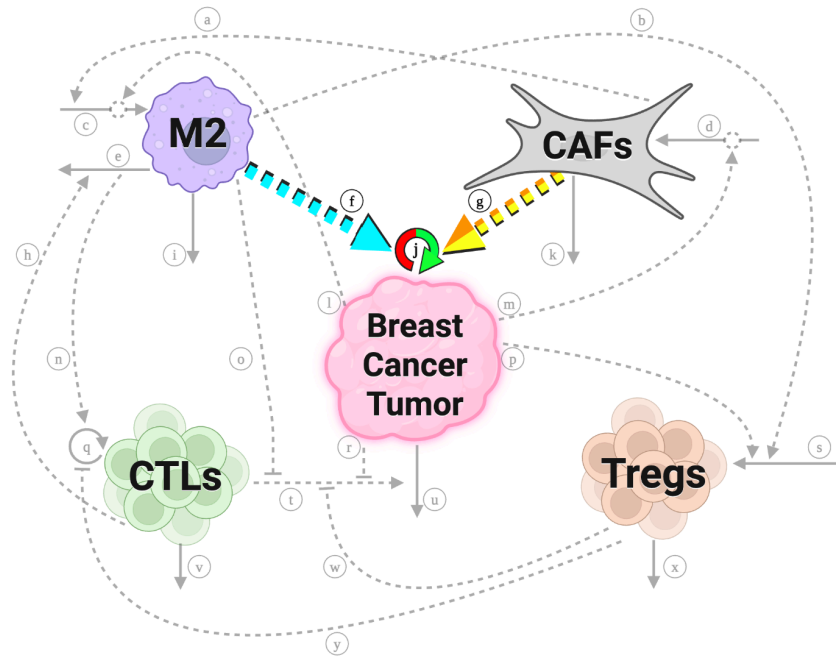


Figure 5. Heatmap of sensitivity analysis results. Caption: Our model diagram with important pathways highlighted. Important pathways are highlighted according to a rainbow heatmap of descending level of influence. Red indicates the pathway that contains the most-important parameter in our model, orange indicates the pathway with the second-most parameter , etc. **Pathway j** is split into two colors, as the most-influential parameter, p_B , and the fourth most-influential parameter, K_B , are both in **pathway j**. Similarly, **pathway g** is split into two colors, as the second most-influential parameter, α_{FB} , and the third most-influential parameter, β_{FB} , are both in **pathway g**. The fifth most-influential parameter, α_{2B} , is in **pathway f**. Figure created with Biorender.com

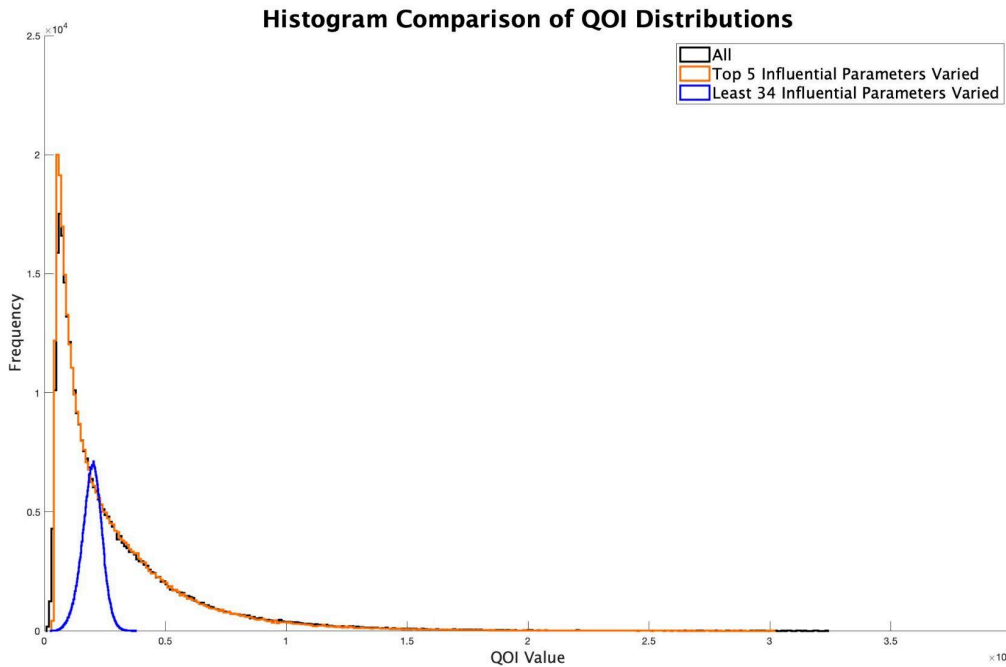


Figure 6. Histograms showing distribution of QoI values when various sets of parameters are allowed to vary. Caption: To compare model behavior produced by all parameters versus model behavior produced by the top six most-influential parameters, we first let all 39 parameters vary and calculated the QoI using each of the 175,000 parameter sets used in the global sensitivity analysis. The black curve is a histogram of QoI values produced by letting all parameters vary. The orange curve is a histogram of QoI values produced by only letting the top six most-influential parameters vary, while the 34 least-influential parameters remain fixed at their nominal values. For contrast, the blue curve is a histogram of QoI values produced by only letting the 34 least-influential parameters vary, and freezing the top 5. The variability in the QoI when the top five most-influential parameters are varied closely aligns with the QoI variability when all of the parameters are varied.

The sensitivity analysis results are useful for indicating which parameters have more influence than others, but they do not elucidate specific relationships between certain parameters. To show these relationships, we plotted each possible pair of the top five most-influential parameters and colored each point in the plot by its QoI value. Specifically, we took a subset of 10,000 parameter sets used for the global sensitivity analysis and the QoI values they produced, and plotted values of one parameter on the horizontal axis, and values of another parameter' on the vertical axis, with each point colored by a heatmap to depict its QoI value. These projections onto two-dimensional planes in parameter space help us understand any patterns that pairs of parameters have on our QoI. For example, in Fig. 7 the top left pairwise plot shows that even if a tumor has a relatively fast proliferation rate, a weak boosting effect from fibroblasts could potentially result in a smaller TNBC tumor. That is, CAFs cytokine secretion represents a potential therapeutic target, even in the context of aggressive tumor growth. This analysis therefore provides insight into which biological interactions may offer the greatest leverage for combination treatment strategies, beyond ranking parameters in isolation

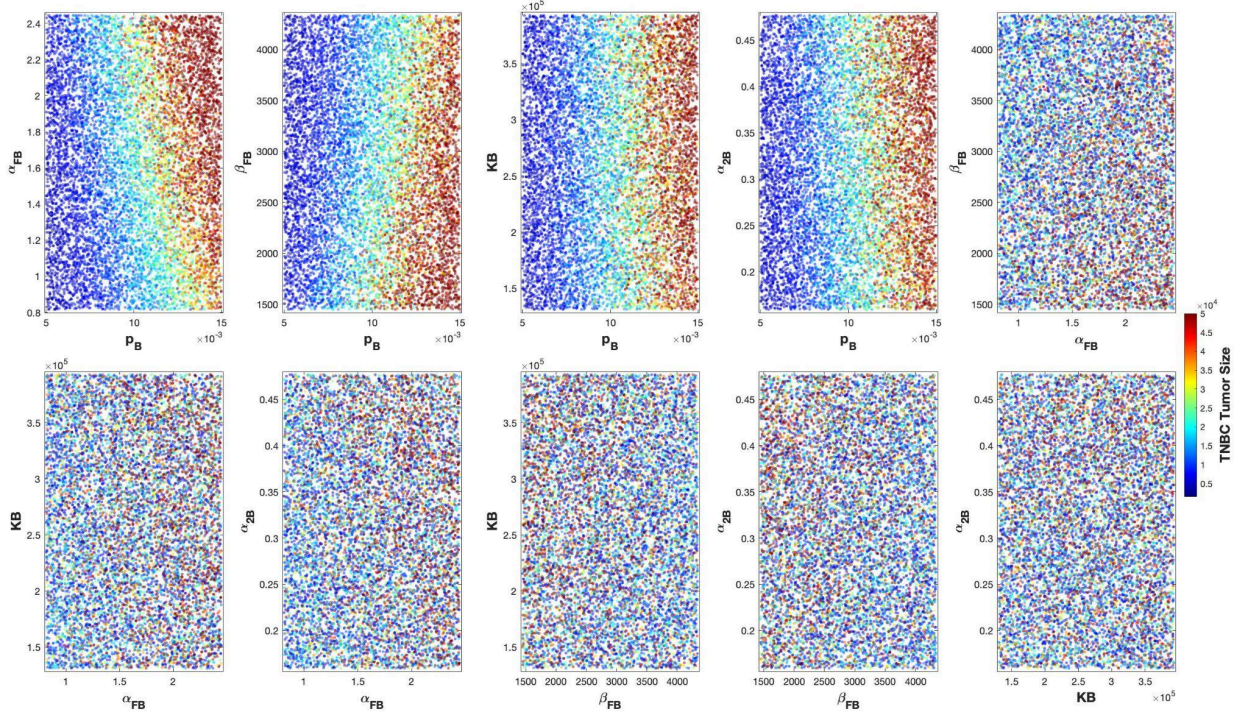


Figure 7. Pairwise relationships between the most influential parameters. Caption: Projection plots in two-dimensional subsets of parameter space, colored by QoI value showing pairwise interactions between the top five most-influential parameters. A subset of 10,000 parameter sets and the corresponding QoI values they produced were randomly selected from those used to perform the global sensitivity analysis. On each plot, two influential parameters were selected for the axes, and each of the 10,000 points were plotted according to their values for those two parameters. The points in each plot are colored according to the size of the QoI those values produced. The colorbar indicates larger QoI values are represented by red, and smaller QoI values are represented by blue. The plots were created with MATLAB 2024b.

Discussion

In this work, we developed a novel ODE model to describe key interactions within the TNBC TME. By modeling five representative cell populations and their dominant interactions, we captured biologically-meaningful dynamics that align with current understanding of TNBC progression and immune evasion. Global sensitivity analysis identified a small subset of parameters that exert a disproportionate influence on tumor burden over a clinically-relevant timeframe.

Notably, the most-influential parameters correspond to pathways involving CAF and M2 macrophage-mediated immune suppression, both of which are increasingly recognized as important contributors to TNBC aggressiveness, and are being investigated as therapeutic targets in clinical studies. While the model does not explicitly simulate therapeutic interventions, the prominence of these pathways supports their relevance as promising areas for future investigation in the context of combination therapies.

In the future, we can mathematically model these current or theoretical therapies using our model to predict expected outcomes for various regimens. We can also use our model and optimal control methods to optimize any combination drug regimens for triple-negative breast cancer patients. Our

rigorous parameter estimations can also be used by other modelers who study different types of breast cancer, other cancers, and other diseases, supporting the wider scientific community.

The primary limitations of this work arise from parameter uncertainty and model reduction. Comprehensive, quantitative data describing immune and stromal dynamics in human TNBC tumors remain limited, necessitating the use of data from related experimental systems and informed estimation for certain parameters. Although these choices introduce uncertainty, the sensitivity analysis explores the behavior of the system with different parameter values, and it provides information on relative influence rather than precise numerical prediction.

Additionally, reducing the TME to five interacting populations necessarily excludes other relevant cell types and signaling pathways. This simplification was required to ensure model identifiability and interpretability. It results in parameters that represent net effects in the system, which includes effects beyond their descriptions, due to the absence of other components that may also be relevant. Future extensions of this work may incorporate experimental data, additional cell populations, or treatment effects.

Bibliography

1. Global cancer burden growing, amidst mounting need for services. World Health Organization. February 1, 2024. Accessed July 11, 2024.
<https://www.who.int/news/item/01-02-2024-global-cancer-burden-growing--amidst-mounting-need-for-services>
2. Triple-negative Breast Cancer | Details, Diagnosis, and Signs. American Cancer Society. March 1, 2023. Accessed July 11, 2024.
<https://www.cancer.org/cancer/types/breast-cancer/about/types-of-breast-cancer/triple-negative.html>
3. Giaquinto AN, Sung H, Miller KD, et al. Breast Cancer Statistics, 2022. *CA Cancer J Clin*. 2022;72(6):524-541. doi:10.3322/caac.21754
4. Fan Y, He S. The Characteristics of Tumor Microenvironment in Triple Negative Breast Cancer. *Cancer Manag Res*. 2022;14:1-17. doi:10.2147/CMAR.S316700
5. Smrekar K, Belyakov A, Jin K. Crosstalk between triple negative breast cancer and microenvironment. *Oncotarget*. 2023;14:284-293. doi:10.18632/oncotarget.28397
6. Garrido JM, Martínez-Rodríguez D, Rodríguez-Serrano F, et al. Mathematical model optimized for prediction and health care planning for COVID-19. *Med Intensiva*. 2022;46(5):248-258. doi:10.1016/j.medine.2022.02.020
7. Mathur D, Barnett E, Scher HI, Xavier JB. Optimizing the future: how mathematical models inform treatment schedules for cancer. *Trends Cancer*. 2022;8(6):506-516. doi:10.1016/j.trecan.2022.02.005
8. Aghaee M, Ledzewicz U, Robbins M, Bezman N, Cho HJ, Moore H. Determining Optimal Combination Regimens for Patients with Multiple Myeloma. *arXiv*. Preprint posted online November 16, 2022. Accessed June 23, 2024. <http://arxiv.org/abs/2211.09280>
9. Yin A, Moes DJAR, van Hasselt JGC, Swen JJ, Guchelaar H. A Review of Mathematical Models for Tumor Dynamics and Treatment Resistance Evolution of Solid Tumors. *CPT Pharmacomet Syst Pharmacol*. 2019;8(10):720-737. doi:10.1002/psp4.12450
10. Vikas P, Borcherding N, Zhang W. The clinical promise of immunotherapy in triple-negative breast cancer. *Cancer Manag Res*. 2018;10:6823-6833. doi:10.2147/CMAR.S185176
11. Akman T, Arendt LM, Geisler J, Kristensen VN, Frigessi A, Köhn-Luque A. Modeling of Mouse Experiments Suggests that Optimal Anti-Hormonal Treatment for Breast Cancer is Diet-Dependent. *Bull Math Biol*. 2024;86(4):42. doi:10.1007/s11538-023-01253-1
12. Schmiester L, Brasó-Maristany F, González-Farré B, et al. Computational Model Predicts Patient Outcomes in Luminal B Breast Cancer Treated with Endocrine Therapy and CDK4/6 Inhibition. *Clin Cancer Res Off J Am Assoc Cancer Res*. 2024;30(17):3779-3787. doi:10.1158/1078-0432.CCR-24-0244
13. Abernathy K, Abernathy Z, Baxter A, Stevens M. Global Dynamics of a Breast Cancer Competition Model. *Differ Equ Dyn Syst*. 2020;28(4):791-805. doi:10.1007/s12591-017-0346-x

14. Sukpol W, Laomettachit T, Tangthanawatsakul A. A Cancer Subpopulation Competition Model Reveals Optimal Levels of Immune Response that Minimize Tumor Size. *J Comput Biol.* 2024;31(11):1179-1194. doi:10.1089/cmb.2024.0618
15. Solís-Pérez JE, Gómez-Aguilar JF, Atangana A. A fractional mathematical model of breast cancer competition model. *Chaos Solitons Fractals.* 2019;127:38-54. doi:10.1016/j.chaos.2019.06.027
16. Chavada A, Pathak N, Raval R. Fractional mathematical modeling of breast cancer stages with true data from Saudi Arabia. *Results Control Optim.* 2024;15:100431. doi:10.1016/j.rico.2024.100431
17. Aldwoah K, Louati H, Eljaneid N, Aljaaidi T, Alqarni F, Elsayed A. Fractional and stochastic modeling of breast cancer progression with real data validation. *PLOS ONE.* 2025;20(1):e0313676. doi:10.1371/journal.pone.0313676
18. Jarrett AM, Bloom MJ, Godfrey W, et al. Mathematical modelling of trastuzumab-induced immune response in an in vivo murine model of HER2+ breast cancer. *Math Med Biol.* 2019;36(3):381-410. doi:10.1093/imammb/dqy014
19. Roe-Dale R, Isaacson D, Kupferschmid M. A Mathematical Model of Breast Cancer Treatment with CMF and Doxorubicin. *Bull Math Biol.* Published online June 8, 2010:585-608. doi:10.1007/s11538-010-9549-9
20. Wei HC. Mathematical modeling of tumor growth and treatment: Triple negative breast cancer. *Math Comput Simul.* 2023;204:645-659. doi:10.1016/j.matcom.2022.09.005
21. Wei HC. Mathematical modeling of ER-positive breast cancer treatment with AZD9496 and palbociclib. *AIMS Math.* 2020;5(4):3446-3455. doi:10.3934/math.2020223
22. Nave O. Asymptotic analysis of mathematical model describing a new treatment of breast cancer using AZD9496 and palbociclib. *Front Oncol.* 2025;14. doi:10.3389/fonc.2024.1482223
23. Mehdizadeh R, Shariatpanahi SP, Goliae B, Peyvandi S, Rüegg C. Dormant Tumor Cell Vaccination: A Mathematical Model of Immunological Dormancy in Triple-Negative Breast Cancer. *Cancers.* 2021;13(2):245. doi:10.3390/cancers13020245
24. Mohammad Mirzaei N, Su S, Sofia D, et al. A Mathematical Model of Breast Tumor Progression Based on Immune Infiltration. *J Pers Med.* 2021;11(10):1031. doi:10.3390/jpm11101031
25. Mirzaei NM, Changizi N, Asadpoure A, et al. Investigating key cell types and molecules dynamics in PyMT mice model of breast cancer through a mathematical model. *PLOS Comput Biol.* 2022;18(3):e1009953. doi:10.1371/journal.pcbi.1009953
26. Arulraj T, Wang H, Emens LA, Santa-Maria CA, Popel AS. A transcriptome-informed QSP model of metastatic triple-negative breast cancer identifies predictive biomarkers for PD-1 inhibition. *Sci Adv.* 9(26):eadg0289. doi:10.1126/sciadv.adg0289
27. Maiti S, Rangarajan A, Kareenahalli V. Experimentally-driven mathematical model to understand the effects of matrix deprivation in breast cancer metastasis. *NPJ Syst Biol Appl.* 2024;10:132. doi:10.1038/s41540-024-00443-4

28. Akil H, Fatmi NI, Hattaf K. Mathematical optimization of breast cancer treatments: analyzing control strategies for hormone therapy, ketogenic diet and immunotherapy. *J Math Comput Sci.* 2025;15(0):Article ID 9. doi:10.28919/10.28919/jmcs/9420

29. Enderling H, Alexander R.A. Anderson, Mark A.J. Chaplain, Alastair J. Munro, Jayant S. Vaidya. Mathematical modelling of radiotherapy strategies for early breast cancer. *J Theor Biol.* 2006;241(1):158-171. doi:<https://doi.org/10.1016/j.jtbi.2005.11.015>

30. Knútsdóttir H, Pálsson E, Edelstein-Keshet L. Mathematical model of macrophage-facilitated breast cancer cells invasion. *J Theor Biol.* 2014;357:184-199. doi:10.1016/j.jtbi.2014.04.031

31. Christenson C, Wu C, Hormuth DA, et al. Personalizing neoadjuvant chemotherapy regimens for triple-negative breast cancer using a biology-based digital twin. *NPJ Syst Biol Appl.* 2025;11:53. doi:10.1038/s41540-025-00531-z

32. Christenson C, Wu C, Hormuth DA, et al. Fast model calibration for predicting the response of breast cancer to chemotherapy using proper orthogonal decomposition. *J Comput Sci.* 2024;82:102400. doi:10.1016/j.jocs.2024.102400

33. Weis JA, Miga MI, Arlinghaus LR, et al. Predicting the Response of Breast Cancer to Neoadjuvant Therapy Using a Mechanically Coupled Reaction-Diffusion Model. *Cancer Res.* 2015;75(22):4697-4707. doi:10.1158/0008-5472.CAN-14-2945

34. Miniere HJM, Lima EABF, Lorenzo G, et al. A mathematical model for predicting the spatiotemporal response of breast cancer cells treated with doxorubicin. *Cancer Biol Ther.* 25(1):2321769. doi:10.1080/15384047.2024.2321769

35. Norton KA, Wallace T, Pandey NB, Popel AS. An agent-based model of triple-negative breast cancer: the interplay between chemokine receptor CCR5 expression, cancer stem cells, and hypoxia. *BMC Syst Biol.* 2017;11(1):68. doi:10.1186/s12918-017-0445-x

36. Qiu X, Zhao T, Luo R, Qiu R, Li Z. Tumor-Associated Macrophages: Key Players in Triple-Negative Breast Cancer. *Front Oncol.* 2022;12:772615. doi:10.3389/fonc.2022.772615

37. Pe KCS, Saetung R, Yodsurang V, et al. Triple-negative breast cancer influences a mixed M1/M2 macrophage phenotype associated with tumor aggressiveness. *PLoS ONE.* 2022;17(8):e0273044. doi:10.1371/journal.pone.0273044

38. Hao M, Huang B, Wu R, Peng Z, Luo KQ. The Interaction between Macrophages and Triple-negative Breast Cancer Cells Induces ROS-Mediated Interleukin 1 α Expression to Enhance Tumorigenesis and Metastasis. *Adv Sci.* 2023;10(29):2302857. doi:10.1002/advs.202302857

39. Yuan ZY, Luo RZ, Peng RJ, Wang SS, Xue C. High infiltration of tumor-associated macrophages in triple-negative breast cancer is associated with a higher risk of distant metastasis. *Oncotargets Ther.* 2014;7:1475-1480. doi:10.2147/OTT.S61838

40. Strizova Z, Benesova I, Bartolini R, et al. M1/M2 macrophages and their overlaps – myth or reality? *Clin Sci Lond Engl* 1979. 2023;137(15):1067-1093. doi:10.1042/CS20220531

41. Wang S, Wang J, Chen Z, et al. Targeting M2-like tumor-associated macrophages is a potential therapeutic approach to overcome antitumor drug resistance. *Npj Precis Oncol*. 2024;8(1):1-19. doi:10.1038/s41698-024-00522-z
42. Shang L, Zhong Y, Yao Y, et al. Subverted macrophages in the triple-negative breast cancer ecosystem. *Biomed Pharmacother*. 2023;166:115414. doi:10.1016/j.biopha.2023.115414
43. Cohen N, Shani O, Raz Y, et al. Fibroblasts drive an immunosuppressive and growth-promoting microenvironment in breast cancer via secretion of Chitinase 3-like 1. *Oncogene*. 2017;36(31):4457-4468. doi:10.1038/onc.2017.65
44. Yu Y, Xiao CH, Tan LD, Wang QS, Li XQ, Feng YM. Cancer-associated fibroblasts induce epithelial–mesenchymal transition of breast cancer cells through paracrine TGF- β signalling. *Br J Cancer*. 2014;110(3):724-732. doi:10.1038/bjc.2013.768
45. Liu J, Chen S, Wang W, et al. Cancer-associated fibroblasts promote hepatocellular carcinoma metastasis through chemokine-activated hedgehog and TGF- β pathways. *Cancer Lett*. 2016;379(1):49-59. doi:10.1016/j.canlet.2016.05.022
46. Laoui D, Movahedi K, Van Overmeire E, et al. Tumor-associated macrophages in breast cancer: distinct subsets, distinct functions. *Int J Dev Biol*. 2011;55(7-8-9):861-867. doi:10.1387/ijdb.113371dl
47. Zhang F, Wang H, Wang X, et al. TGF- β induces M2-like macrophage polarization via SNAIL-mediated suppression of a pro-inflammatory phenotype. *Oncotarget*. 2016;7(32):52294-52306. doi:10.18632/oncotarget.10561
48. Hollmén M, Karaman S, Schwager S, et al. G-CSF regulates macrophage phenotype and associates with poor overall survival in human triple-negative breast cancer. *OncoImmunology*. 2016;5(3):e1115177. doi:10.1080/2162402X.2015.1115177
49. Santoni M, Romagnoli E, Saladino T, et al. Triple negative breast cancer: Key role of Tumor-Associated Macrophages in regulating the activity of anti-PD-1/PD-L1 agents. *Biochim Biophys Acta Rev Cancer*. 2018;1869(1):78-84. doi:10.1016/j.bbcan.2017.10.007
50. Ceeraz S, Nowak EC, Noelle RJ. B7 family checkpoint regulators in immune regulation and disease. *Trends Immunol*. 2013;34(11):556-563. doi:10.1016/j.it.2013.07.003
51. Kuang DM, Zhao Q, Peng C, et al. Activated monocytes in peritumoral stroma of hepatocellular carcinoma foster immune privilege and disease progression through PD-L1. *J Exp Med*. 2009;206(6):1327-1337. doi:10.1084/jem.20082173
52. Wrzesinski SH, Wan YY, Flavell RA. Transforming growth factor- β and the immune response: Implications for anticancer therapy. *Clin Cancer Res*. 2007;13(18):5262-5270. doi:10.1158/1078-0432.CCR-07-1157
53. Huang R, Kang T, Chen S. The role of tumor-associated macrophages in tumor immune evasion. *J Cancer Res Clin Oncol*. 2024;150(5):238. doi:10.1007/s00432-024-05777-4

54. Zhou T, Qian H, Zhang D, et al. PGRN inhibits CD8+T cell recruitment and promotes breast cancer progression by up-regulating ICAM-1 on TAM. *Cancer Immunol Immunother.* 2024;73(5):76. doi:10.1007/s00262-024-03655-z

55. Ochoa JB, Strange J, Kearney P, Gellin G, Endean E, Fitzpatrick E. Effects of L-Arginine on the Proliferation of T Lymphocyte Subpopulations. *J Parenter Enter Nutr.* 2001;25(1):23-29. doi:10.1177/014860710102500123

56. Rodriguez PC, Zea AH, DeSalvo J, et al. L-Arginine Consumption by Macrophages Modulates the Expression of CD3 ζ Chain in T Lymphocytes. *J Immunol.* 2003;171(3):1232-1239. doi:10.4049/jimmunol.171.3.1232

57. Chen Y, Shu X, Guo JY, et al. Nanodrugs mediate TAMs-related arginine metabolism interference to boost photodynamic immunotherapy. *J Controlled Release.* 2024;367:248-264. doi:10.1016/j.jconrel.2024.01.045

58. Smyth MJ, Strobl SL, Young HA, Ortaldo JR, Ochoa AC. Regulation of lymphokine-activated killer activity and pore-forming protein gene expression in human peripheral blood CD8+ T lymphocytes. Inhibition by transforming growth factor-beta. *J Immunol.* 1991;146(10):3289-3297. doi:10.4049/jimmunol.146.10.3289

59. Adalid-Peralta L, Fragoso G, Fleury A, Sciuotto E. Mechanisms Underlying the Induction of Regulatory T cells and Its Relevance in the Adaptive Immune Response in Parasitic Infections. *Int J Biol Sci.* 2011;7(9):1412-1426.

60. Curiel TJ, Coukos G, Zou L, et al. Specific recruitment of regulatory T cells in ovarian carcinoma fosters immune privilege and predicts reduced survival. *Nat Med.* 2004;10(9):942-949. doi:10.1038/nm1093

61. Anand N, Peh KH, Kolesar JM. Macrophage Repolarization as a Therapeutic Strategy for Osteosarcoma. *Int J Mol Sci.* 2023;24(3):2858. doi:10.3390/ijms24032858

62. Chaudhary A, Patil P, Raina P, Kaul-Ghanekar R. Matairesinol repolarizes M2 macrophages to M1 phenotype to induce apoptosis in triple-negative breast cancer cells. *Immunopharmacol Immunotoxicol.* 2025;47(1):8-22. doi:10.1080/08923973.2024.2425028

63. Medina MA, Oza G, Sharma A, et al. Triple-Negative Breast Cancer: A Review of Conventional and Advanced Therapeutic Strategies. *Int J Environ Res Public Health.* 2020;17(6):2078. doi:10.3390/ijerph17062078

64. Yang D, Liu J, Qian H, Zhuang Q. Cancer-associated fibroblasts: from basic science to anticancer therapy. *Exp Mol Med.* 2023;55(7):1322-1332. doi:10.1038/s12276-023-01013-0

65. Hu D, Li Z, Zheng B, et al. Cancer-associated fibroblasts in breast cancer: Challenges and opportunities. *Cancer Commun.* 2022;42(5):401-434. doi:10.1002/cac2.12291

66. Takai K, Le A, Weaver VM, Werb Z. Targeting the cancer-associated fibroblasts as a treatment in triple-negative breast cancer. *Oncotarget.* 2016;7(50):82889-82901. doi:10.18632/oncotarget.12658

67. Orimo A, Gupta PB, Sgroi DC, et al. Stromal Fibroblasts Present in Invasive Human Breast Carcinomas Promote Tumor Growth and Angiogenesis through Elevated SDF-1/CXCL12 Secretion. *Cell*. 2005;121(3):335-348. doi:10.1016/j.cell.2005.02.034

68. Wang G, Zhang H, Shen X, Jin W, Wang X, Zhou Z. Characterization of cancer-associated fibroblasts (CAFs) and development of a CAF-based risk model for triple-negative breast cancer. *Cancer Cell Int*. 2023;23(1):294. doi:10.1186/s12935-023-03152-w

69. Wang M, Feng R, Chen Z, et al. Identification of Cancer-Associated Fibroblast Subtype of Triple-Negative Breast Cancer. *J Oncol*. 2022;2022:6452636. doi:10.1155/2022/6452636

70. Sarkar M, Nguyen T, Gundre E, et al. Cancer-associated fibroblasts: The chief architect in the tumor microenvironment. *Front Cell Dev Biol*. 2023;11:1089068. doi:10.3389/fcell.2023.1089068

71. Zhou J, Wang XH, Zhao YX, et al. Cancer-Associated Fibroblasts Correlate with Tumor-Associated Macrophages Infiltration and Lymphatic Metastasis in Triple Negative Breast Cancer Patients. *J Cancer*. 2018;9(24):4635-4641. doi:10.7150/jca.28583

72. Xian P, Zou L, Zhang J, et al. Precision targeted cancer-associated fibroblast nano-regulator enhanced chemo-immunotherapy for triple-negative breast cancer. *Biomaterials*. 2026;326:123679. doi:10.1016/j.biomaterials.2025.123679

73. Kansy BA, Concha-Benavente F, Srivastava RM, et al. PD-1 status in CD8+ T cells associates with survival and anti-PD-1 therapeutic outcomes in head and neck cancer. *Cancer Res*. 2017;77(22):6353-6364. doi:10.1158/0008-5472.CAN-16-3167

74. Jia H, Truica CI, Wang B, et al. Immunotherapy for triple-negative breast cancer: Existing challenges and exciting prospects. *Drug Resist Updat*. 2017;32:1-15. doi:10.1016/j.drup.2017.07.002

75. Martínez-Lostao L, Anel A, Pardo J. How Do Cytotoxic Lymphocytes Kill Cancer Cells? *Clin Cancer Res*. 2015;21(22):5047-5056. doi:10.1158/1078-0432.CCR-15-0685

76. Wimberly H, Brown JR, Schalper K, et al. PD-L1 expression correlates with tumor-infiltrating lymphocytes and response to neoadjuvant chemotherapy in breast cancer. *Cancer Immunol Res*. 2015;3(4):326-332. doi:10.1158/2326-6066.CIR-14-0133

77. Noubissi Nzeteu GA, Schlichtner S, David S, et al. Macrophage Differentiation and Polarization Regulate the Release of the Immune Checkpoint Protein V-Domain Ig Suppressor of T Cell Activation. *Front Immunol*. 2022;13:837097. doi:10.3389/fimmu.2022.837097

78. Fan X, Quezada SA, Sepulveda MA, Sharma P, Allison JP. Engagement of the ICOS pathway markedly enhances efficacy of CTLA-4 blockade in cancer immunotherapy. *J Exp Med*. 2014;211(4):715-725. doi:10.1084/jem.20130590

79. Sharma N, Fan X, Atolagbe OT, et al. ICOS costimulation in combination with CTLA-4 blockade remodels tumor-associated macrophages toward an antitumor phenotype. *J Exp Med*. 2024;221(4):e20231263. doi:10.1084/jem.20231263

80. Macallan DC, Wallace D, Zhang Y, et al. Rapid Turnover of Effector-Memory CD4+ T Cells in Healthy Humans. *J Exp Med*. 2004;200(2):255-260. doi:10.1084/jem.20040341

81. Huang P, Zhou X, Zheng M, Yu Y, Jin G, Zhang S. Regulatory T cells are associated with the tumor immune microenvironment and immunotherapy response in triple-negative breast cancer. *Front Immunol.* 2023;14. doi:10.3389/fimmu.2023.1263537
82. Malla RR, Vasudevaraju P, Vempati RK, Rakshmitha M, Merchant N, Nagaraju GP. Regulatory T cells: Their role in triple-negative breast cancer progression and metastasis. *Cancer.* 2022;128(6):1171-1183. doi:10.1002/cncr.34084
83. Zahran AM, El-Badawy O, Kamel LM, Rayan A, Rezk K, Abdel-Rahim MH. Accumulation of Regulatory T Cells in Triple Negative Breast Cancer Can Boost Immune Disruption. *Cancer Manag Res.* 2021;13:6019-6029. doi:10.2147/CMAR.S285128
84. Vukmanovic-Stejic M, Zhang Y, Cook JE, et al. Human CD4+ CD25hi Foxp3+ regulatory T cells are derived by rapid turnover of memory populations in vivo. *J Clin Invest.* 2006;116(9):2423-2433. doi:10.1172/JCI28941
85. Whiteside TL. The role of regulatory T cells in cancer immunology. *Immunotargets Ther.* 2015;4:159-171. doi:10.2147/ITT.S55415
86. Taylor NA, Vick SC, Iglesia MD, et al. Treg depletion potentiates checkpoint inhibition in claudin-low breast cancer. *J Clin Invest.* 2017;127(9):3472-3483. doi:10.1172/JCI90499
87. Chang LY, Lin YC, Mahalingam J, et al. Tumor-derived chemokine CCL5 enhances TGF- β -mediated killing of CD8(+) T cells in colon cancer by T-regulatory cells. *Cancer Res.* 2012;72(5):1092-1102. doi:10.1158/0008-5472.CAN-11-2493
88. Qiu J, Xu L, Zeng X, et al. CCL5 mediates breast cancer metastasis and prognosis through CCR5/Treg cells. *Front Oncol.* 2022;12. doi:10.3389/fonc.2022.972383
89. Yu T, Di G. Role of tumor microenvironment in triple-negative breast cancer and its prognostic significance. *Chin J Cancer Res.* 2017;29(3):237-252. doi:10.21147/j.issn.1000-9604.2017.03.10
90. Sawant DV, Yano H, Chikina M, et al. Adaptive plasticity of IL-10+ and IL-35+ Treg cells cooperatively promotes tumor T cell exhaustion. *Nat Immunol.* 2019;20(6):724-735. doi:10.1038/s41590-019-0346-9
91. McNally A, Hill GR, Sparwasser T, Thomas R, Steptoe RJ. CD4+CD25+ regulatory T cells control CD8+ T-cell effector differentiation by modulating IL-2 homeostasis. *Proc Natl Acad Sci U S A.* 2011;108(18):7529-7534. doi:10.1073/pnas.1103782108
92. Tay C, Tanaka A, Sakaguchi S. Tumor-infiltrating regulatory T cells as targets of cancer immunotherapy. *Cancer Cell.* 2023;41(3):450-465. doi:10.1016/j.ccr.2023.02.014
93. Tzikas AK, Nemes S, Linderholm BK. A comparison between young and old patients with triple-negative breast cancer: biology, survival and metastatic patterns. *Breast Cancer Res Treat.* 2020;182(3):643-654. doi:10.1007/s10549-020-05727-x
94. Gradishar WJ, Moran MS, Abraham J, et al. NCCN Guidelines® Insights: Breast Cancer, Version 5.2025: Featured Updates to the NCCN Guidelines. *J Natl Compr Canc Netw.* 2025;23(11):426-436. doi:10.6004/jnccn.2025.0053

95. Tarique AA, Logan J, Thomas E, Holt PG, Sly PD, Fantino E. Phenotypic, Functional, and Plasticity Features of Classical and Alternatively Activated Human Macrophages. *Am J Respir Cell Mol Biol.* 2015;53(5):676-688. doi:10.1165/rcmb.2015-0012OC

96. Sezginer O, Unver N. Dissection of pro-tumoral macrophage subtypes and immunosuppressive cells participating in M2 polarization. *Inflamm Res.* 2024;73(9):1411-1423. doi:10.1007/s00011-024-01907-3

97. Xiao H, Guo Y, Li B, et al. M2-Like Tumor-Associated Macrophage-Targeted Codelivery of STAT6 Inhibitor and IKK β siRNA Induces M2-to-M1 Repolarization for Cancer Immunotherapy with Low Immune Side Effects. *ACS Cent Sci.* 2020;6(7):1208-1222. doi:10.1021/acscentsci.9b01235

98. Le Mercier I, Chen W, Lines JL, et al. VISTA Regulates the Development of Protective Antitumor Immunity. *Cancer Res.* 2014;74(7):1933-1944. doi:10.1158/0008-5472.CAN-13-1506

99. Qin W, Chen B, Li X, et al. Cancer-associated fibroblasts secrete CSF3 to promote TNBC progression via enhancing PGM2L1-dependent glycolysis reprogramming. *Cell Death Dis.* 2025;16(1):249. doi:10.1038/s41419-025-07580-6

100. Fan C, Zhu W, Chen Y, Zhu W, Ding J. Cancer-Associated Fibroblasts: Origin, Classification, Tumorigenicity, and Targeting for Cancer Therapy. *MedComm.* 2025;6(11):e70415. doi:10.1002/mco2.70415

101. Heesterman BL, Bokhorst JM, de Pont LMH, et al. Mathematical Models for Tumor Growth and the Reduction of Overtreatment. *J Neurol Surg Part B Skull Base.* 2019;80(1):72-78. doi:10.1055/s-0038-1667148

102. Zhang C, Fei Y, Wang H, et al. CAFs orchestrates tumor immune microenvironment—A new target in cancer therapy? *Front Pharmacol.* 2023;14:1113378. doi:10.3389/fphar.2023.1113378

103. Qiu X, Zhao T, Luo R, Qiu R, Li Z. Tumor-Associated Macrophages: Key Players in Triple-Negative Breast Cancer. *Front Oncol.* 2022;12:772615. doi:10.3389/fonc.2022.772615

104. Alkaabi D, Arafat K, Sulaiman S, Al-Azawi AM, Attoub S. PD-1 Independent Role of PD-L1 in Triple-Negative Breast Cancer Progression. *Int J Mol Sci.* 2023;24(7):6420. doi:10.3390/ijms24076420

105. Kaech SM, Wherry EJ, Ahmed R. Effector and memory T-cell differentiation: implications for vaccine development. *Nat Rev Immunol.* 2002;2(4):251-262. doi:10.1038/nri778

106. Jr CAJ, Travers P, Walport M, et al. *Immunobiology*. 5th ed. Garland Science; 2001.

107. Tomioka H, Tatano Y, Maw WW, Sano C, Kanehiro Y, Shimizu T. Characteristics of Suppressor Macrophages Induced by Mycobacterial and Protozoal Infections in relation to Alternatively Activated M2 Macrophages. *Clin Dev Immunol.* 2012;2012:635451. doi:10.1155/2012/635451

108. Otterlei Fjørtoft M, Huse K, Rye IH. The Tumor Immune Microenvironment in Breast Cancer Progression. *Acta Oncol Stockh Swed.* 2024;63:359-367. doi:10.2340/1651-226X.2024.33008

109. Hunter M, Wang Y, Eubank T, Baran C, Nana-Sinkam P, Marsh C. Survival of monocytes and macrophages and their role in health and disease. *Front Biosci J Virtual Libr.* 2009;14:4079-4102. doi:10.2741/3514

110. Lee SH, Kim YS, Han W, et al. Tumor growth rate of invasive breast cancers during wait times for surgery assessed by ultrasonography. *Medicine (Baltimore).* 2016;95(37):e4874. doi:10.1097/MD.0000000000004874

111. Elfoly M, Mirza JY, Alaiya A, et al. PD-L1 intrinsically promotes the proliferation of breast cancer cells through the SKP2-p27/p21 axis. *Cancer Cell Int.* 2024;24(1):161. doi:10.1186/s12935-024-03354-w

112. D'Arcangelo E, Wu NC, Cadavid JL, McGuigan AP. The life cycle of cancer-associated fibroblasts within the tumour stroma and its importance in disease outcome. *Br J Cancer.* 2020;122(7):931-942. doi:10.1038/s41416-019-0705-1

113. Huang P, Zhou X, Zheng M, Yu Y, Jin G, Zhang S. Regulatory T cells are associated with the tumor immune microenvironment and immunotherapy response in triple-negative breast cancer. *Front Immunol.* 2023;14:1263537. doi:10.3389/fimmu.2023.1263537

114. Mahacek ML, Beer DG, Frank TS, Ethier SP. Finite proliferative lifespan in vitro of a human breast cancer cell strain isolated from a metastatic lymph node. *Breast Cancer Res Treat.* 1993;28(3):267-276. doi:10.1007/BF00666588

115. Guo S, Liu X, Zhang J, et al. Integrated analysis of single-cell RNA-seq and bulk RNA-seq unravels T cell-related prognostic risk model and tumor immune microenvironment modulation in triple-negative breast cancer. *Comput Biol Med.* 2023;161:107066. doi:10.1016/j.combiomed.2023.107066

116. Sun X, Qu Q, Lao Y, et al. Tumor suppressor HIC1 is synergistically compromised by cancer-associated fibroblasts and tumor cells through the IL-6/pSTAT3 axis in breast cancer. *BMC Cancer.* 2019;19(1):1180. doi:10.1186/s12885-019-6333-6

117. Hagenaars SC, Vangangelt KMH, Van Pelt GW, et al. Standardization of the tumor-stroma ratio scoring method for breast cancer research. *Breast Cancer Res Treat.* 2022;193(3):545-553. doi:10.1007/s10549-022-06587-3

118. Narod SA, Iqbal J, Jakubowska A, et al. Are two-centimeter breast cancers large or small? *Curr Oncol.* 2013;20(4):205-211. doi:10.3747/co.20.1364

119. Byrd BK, Krishnaswamy V, Gui J, et al. The Shape of Breast Cancer. *Breast Cancer Res Treat.* 2020;183(2):403-410. doi:10.1007/s10549-020-05780-6

120. Palmer L, Briggs C, McFadden S, et al. ICSH recommendations for the standardization of nomenclature and grading of peripheral blood cell morphological features. *Int J Lab Hematol.* 2015;37(3):287-303. doi:10.1111/ijlh.12327

121. Cano RLE, Lopera HDE. Introduction to T and B lymphocytes. In: *Autoimmunity: From Bench to Bedside [Internet]*. El Rosario University Press; 2013. Accessed December 15, 2025. <https://www.ncbi.nlm.nih.gov/books/NBK459471/>

122. Leonard F, Curtis LT, Yesantharao P, et al. Enhanced performance of macrophage-encapsulated nanoparticle albumin-bound-paclitaxel in hypo-perfused cancer lesions. *Nanoscale*. 2016;8(25):12544-12552. doi:10.1039/c5nr07796f

123. Tu D, Dou J, Wang M, Zhuang H, Zhang X. M2 macrophages contribute to cell proliferation and migration of breast cancer. *Cell Biol Int*. 2021;45(4):831-838. doi:10.1002/cbin.11528

124. Khazen R, Müller S, Lafouresse F, Valitutti S, Cussat-Blanc S. Sequential adjustment of cytotoxic T lymphocyte densities improves efficacy in controlling tumor growth. *Sci Rep*. 2019;9(1):12308. doi:10.1038/s41598-019-48711-2

125. Jin S, Liu W, He X, et al. VISTA deficiency exerts anti-tumor effects in breast cancer through regulating macrophage polarization. *Int Immunopharmacol*. 2024;136:112365. doi:10.1016/j.intimp.2024.112365

126. Shi Z, Du Q, Wang X, et al. Granzyme B in circulating CD8+ T cells as a biomarker of immunotherapy effectiveness and disability in neuromyelitis optica spectrum disorders. *Front Immunol*. 2022;13:1027158. doi:10.3389/fimmu.2022.1027158

127. Abudula M, Astuti Y, Raymant M, Sharma V, Schmid MC, Mielgo A. Macrophages suppress CD8+ T cell cytotoxic function in triple negative breast cancer via VISTA. *Br J Cancer*. 2025;133(1):40-51. doi:10.1038/s41416-025-03013-5

128. Chen ML, Pittet MJ, Gorelik L, et al. Regulatory T cells suppress tumor-specific CD8 T cell cytotoxicity through TGF- β signals in vivo. *Proc Natl Acad Sci*. 2005;102(2):419-424. doi:10.1073/pnas.0408197102

129. Kaneda MM, Messer KS, Ralainirina N, et al. PI3K γ is a molecular switch that controls immune suppression. *Nature*. 2016;539(7629):437-442. doi:10.1038/nature19834

130. Feinerman O, Jentsch G, Tkach KE, et al. Single-cell quantification of IL-2 response by effector and regulatory T cells reveals critical plasticity in immune response. *Mol Syst Biol*. 2010;6(1):MSB201090. doi:10.1038/msb.2010.90

131. Semba T, Wang X, Xie X, et al. Identification of the JNK-Active Triple-Negative Breast Cancer Cluster Associated With an Immunosuppressive Tumor Microenvironment. *JNCI J Natl Cancer Inst*. 2021;114(1):97-108. doi:10.1093/jnci/djab128

132. Chen JH, Agrawal G, Feig B, et al. Triple-negative breast cancer: MRI features in 29 patients. *Ann Oncol*. 2007;18(12):2042-2043. doi:10.1093/annonc/mdm504

133. Kimmelman AC, Sherman MH. The role of stroma in cancer metabolism. *Cold Spring Harb Perspect Med*. 2024;14(5):a041540. doi:10.1101/cshperspect.a041540

134. De Boer RJ, Homann D, Perelson AS. Different dynamics of CD4+ and CD8+ T cell responses during and after acute lymphocytic choriomeningitis virus infection. *J Immunol Baltim Md 1950*. 2003;171(8):3928-3935. doi:10.4049/jimmunol.171.8.3928

135. Shanahan SL, Kunder N, Inaku C, et al. Longitudinal intravascular antibody labeling identified Treg recruitment as a therapeutic target in a mouse model of lung cancer. *J Immunol Baltim Md 1950*. 2024;213(6):906-918. doi:10.4049/jimmunol.2400268

136.Irvin CG, Bates JH. Measuring the lung function in the mouse: the challenge of size. *Respir Res.* 2003;4(1):4. doi:10.1186/rr199

137.Eftimie R, Barelle C. Mathematical investigation of innate immune responses to lung cancer: The role of macrophages with mixed phenotypes. *J Theor Biol.* 2021;524:110739. doi:10.1016/j.jtbi.2021.110739

138.Weissman-Shomer P, Fry M. Chick embryo fibroblasts senescence *in vitro*: Pattern of cell division and life span as a function of cell density. *Mech Ageing Dev.* 1975;4:159-166. doi:10.1016/0047-6374(75)90017-2

139.Cords L, Tietscher S, Anzeneder T, et al. Cancer-associated fibroblast classification in single-cell and spatial proteomics data. *Nat Commun.* 2023;14(1):4294. doi:10.1038/s41467-023-39762-1

140.Soon PSH, Kim E, Pon CK, et al. Breast cancer-associated fibroblasts induce epithelial-to-mesenchymal transition in breast cancer cells. *Endocr Relat Cancer.* 2013;20(1):1-12. doi:10.1530/ERC-12-0227

141.Sobol' IM. Global sensitivity indices for nonlinear mathematical models and their Monte Carlo estimates. *Math Comput Simul.* 2001;55(1):271-280. doi:10.1016/S0378-4754(00)00270-6

142.Saltelli A, Annoni P, Azzini I, Campolongo F, Ratto M, Tarantola S. Variance based sensitivity analysis of model output. Design and estimator for the total sensitivity index. *Comput Phys Commun.* 2010;181(2):259-270. doi:10.1016/j.cpc.2009.09.018